Accepted Manuscript

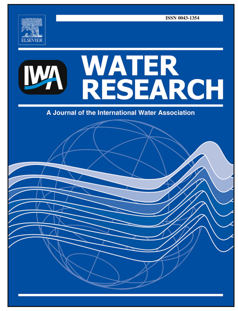

Artificial neural networks as emulators of process-based models to analyse bathing water quality in estuaries

Javier García-Alba, Javier F. Bárcena, Carlos Ugarteburu, Andrés García

PII: S0043-1354(18)30992-8

DOI: https://doi.org/10.1016/j.watres.2018.11.063

Reference: WR 14270

To appear in: *Water Research*

Received Date: 24 July 2018

Revised Date: 26 October 2018

Accepted Date: 21 November 2018

Please cite this article as: García-Alba, J., Bárcena, J.F., Ugarteburu, C., García, A., Artificial neural networks as emulators of process-based models to analyse bathing water quality in estuaries, *Water Research*, https://doi.org/10.1016/j.watres.2018.11.063.

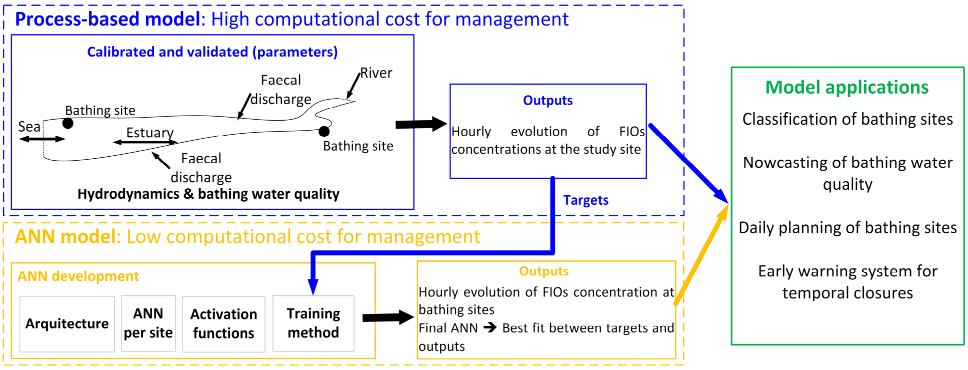

Process-based model: High computational cost for management
Calibrated and validated (parameters)
Faecal discharge
River
Bathing site
Sea
Estuary
Bathing site
Faecal discharge
Hydrodynamics & bathing water quality
Outputs
Hourly evolution of FIOs concentrations at the study site
Targets
ANN model: Low computational cost for management
ANN development
Arquitecture
ANN per site
Activation functions
Training method
Outputs
Hourly evolution of FIOs concentration at bathing sites
Final ANN → Best fit between targets and outputs
Model applications
Classification of bathing sites
Nowcasting of bathing water quality
Daily planning of bathing sites
Early warning system for temporal closures

Artificial neural networks as emulators of process-based models to analyse bathing water quality in estuaries

Javier García-Alba[1,*], Javier F. Bárcena[1], Carlos Ugarteburu[1], Andrés García[1]

[1] *Environmental Hydraulics Institute "IHCantabria", Universidad de Cantabria - Isabel Torres, 15, Parque Científico y Tecnológico de Cantabria, 39011, Santander, Spain.*

[*] Corresponding author. E-mail addresses: garciajav@unican.es (Javier García-Alba); barcenajf@unican.es (Javier F. Bárcena); c.ugarteburu@gmail.com (Carlos Ugarteburu); garciagan@unican.es (Andrés García).

Highlights

- The method integrates laboratory analyses, numerical modelling and machine learning.
- ANN configuration for predicting *E. coli* concentration in estuaries is determined.
- ANNs are viable emulators of process-based models driven by highly variable forcing.
- The longer forecasting, the greater the reduction in computational time using ANN.
- Real-time management of bathing water quality is enabled by using ANNs.

Abstract

This study aims to provide a method for developing artificial neural networks in estuaries as emulators of process-based models to analyse bathing water quality and its variability over time and space. The methodology forecasts the concentration of faecal indicator organisms, integrating the accuracy and reliability of field measurements, the spatial and temporal resolution of process-based modelling, and the decrease in computational costs by artificial neural networks whilst preserving the accuracy of results. Thus, the overall approach integrates a coupled hydrodynamic-bacteriological model previously calibrated with field data at the bathing sites into a low-order emulator by using artificial neural networks, which are trained by the process-based model outputs. The application of the method to the Eo Estuary, located on the northwestern coast of Spain, demonstrated that artificial neural networks are viable surrogates of highly nonlinear process-based models and highly variable forcings. The results showed that the process-based model and the neural networks conveniently reproduced the measurements of *Escherichia coli* (*E. coli*) concentrations, indicating a slightly better fit for the process-based model (R^2=0.87) than for the neural networks (R^2=0.83). This application also highlighted that during the model setup of both predictive tools, the computational time of the process-based approach was 0.78 times lower than that of the artificial neural networks (ANNs) approach due to the additional time spent on ANN development. Conversely, the computational costs of forecasting are considerably reduced by the neural networks compared with the process-based model, with a decrease in hours of 25, 600, 3900, and 31633 times for forecasting 1 h 1 day, 1 month and 1 bathing season, respectively. Therefore, the longer the forecasting period, the greater the reduction in computational time by artificial neural networks.

Keywords

Bathing water quality; *Escherichia coli* (*E. coli*); Hydrodynamic-bacteriological model; Machine learning; Eo Estuary

1. Introduction

Estuarine water quality is strongly impacted by anthropogenic activities (García et al., 2010; De los Ríos et al., 2016; Bárcena et al. 2017a). For instance, people are very concerned about bathing water quality since estuarine waters are used not only for recreational activities but also for others including transport and food production and as a repository for sewage and industrial waste (Bárcena et al. 2017b). Therefore, faecal pollution is one of the most relevant issues in the evaluation and management of estuarine water quality since it may cause socio-economic and environmental losses such as infections and diseases, beach degradation, or closures of shellfish-growing areas (de Brauwere et al., 2014).

In Europe, Directive (2006/7/EC) sets the quality of bathing waters based on two faecal indicator organisms (FIOs*): intestinal Enterococci* (*Enterococci*) and *Escherichia coli* (*E. coli*). The limit values of *E. coli* for transitional waters are 250 *E. coli*/100 ml (excellent quality) and 500 *E. coli*/100 ml (good quality) based upon a 95th percentile evaluation and 500 *E. coli*/100 ml (sufficient quality) based upon a 90th percentile evaluation. Although laboratory analyses are the most accurate and reliable methods for evaluating water quality, they require between 24 and 48 h to provide results (Rompré et al., 2002); as a result, the public may be exposed to elevated FIO concentrations during the time required to produce an analytical result. Furthermore, these samples are usually collected either 8 h to 13 h, neglecting the influence of diurnal variation in FIO concentration (Boehm et al., 2002; Thoe et al., 2014). Thus, environmental managers are not able to evaluate faecal pollution variability over time. Although these issues could be overcome by increasing the temporal resolution and window of sampling, the time-consuming laboratory methods will continue to be a bottleneck for the rapid detection of critical conditions such as pollution events.

Therefore, real-time methods have been developed to monitor *E. coli* concentrations based on flow cytometry (Besmer et al., 2014), ATP assays (Vang et al., 2014), online optical sensors (Højris et al., 2016), or quantitative PCR (Walker et al., 2017). However, the current high costs associated with these methods are a drawback to their implementation at bathing sites for most health administrations.

Process-based models have also been used to evaluate the spatial and temporal evolution of FIOs, considering the diurnal variation in FIO concentration (López et al., 2013; Bedri et al., 2014; Wang et al., 2016; Huang et al., 2017). Notwithstanding the increase in computer power, process-based model complexity is also growing at the same rate, if not faster (Washington et al., 2009), suggesting that computational requirements will be an impediment to applications where a quick answer is required, e.g., the nowcasting of FIO concentrations for managing temporal closures of bathing sites.

Accordingly, different techniques have been proposed in the last few years to overcome the large computational burden associated with process-based models, called dynamic emulation modelling (Castelletti et al., 2012). An emulator is a computationally efficient low-order model identified from the original large model and then used to replace it for computationally intensive applications. In the field of bathing water quality monitoring, data-based models such as ANNs may efficiently detect and analyse FIO concentrations and, hence, serve as surrogates for computationally demanding water quality models (Tufail et al., 2008; Shaw et al. 2017). Thus, ANNs may help reduce the computational costs of bathing water quality management, preserving the accuracy of results when large datasets are available for model fitting (van der Merwe et al., 2007; Maier et al., 2010; Shaw et al. 2017). ANNs have been used for nowcasting and forecasting of FIO concentrations in rivers (Chandramouli et al., 2007; Tufail et al., 2008; Motamarri and Boccelli, 2012), reservoirs (Mas and Ahlfeld, 2007), coastal areas (He and He, 2008; Thoe et al., 2012; Thoe et al., 2014; Zhang et al., 2015), and surface runoff (Kim et al., 2008; Kazemi Yazdi and Scholz, 2010). However, their application as emulators of process-based models in estuaries has not been widely investigated.

Within this context, the main objective of this study is to develop a method to compute the spatial and temporal evolution of FIO concentrations in estuaries using ANNs trained by a calibrated hydrodynamic-bacteriological model. This method integrates the benefits of the three approaches used to calculate *E. coli* concentrations: (1) the accuracy and reliability of field measurements; (2) the spatial and temporal resolution of numerical modelling; and (3) the decrease in computational costs caused by ANNs accompanied by preserved accuracy of the results.

2. Material and methods

2.1. Study area and available data

The Eo Estuary (see Fig. 1), located on the northwestern coast of Spain (43º28'33'N; 7º00'03'W), is a shallow mesotidal system with a semidiurnal tidal range varying from 1.2 m to 4.8 m (de Paz et al., 2008). This estuary has been historically divided into two regions. The first region, extending from the estuarine mouth to Vegadeo, presents an N-S alignment over a length of 9.9 km and an average width of 800 m (Flor et al., 1993). The second region, extending from Vegadeo to San Tirso de Abres (FG1), presents NNE-SSW alignment over a length of 4.5 km and a width varying from 95 to 571 m (Flor et al., 1993). The Eo River Basin occupies a catchment area of 819 km^2 with a length of 9 km. The freshwater inflow under natural conditions varies from approximately 0.6 to 425 m^3/s, with an annual average of 19.61 m^3/s and ranging from 7.93 m^3/s in summer to 39.67 m^3/s in winter (Piedracoba et al., 2005).

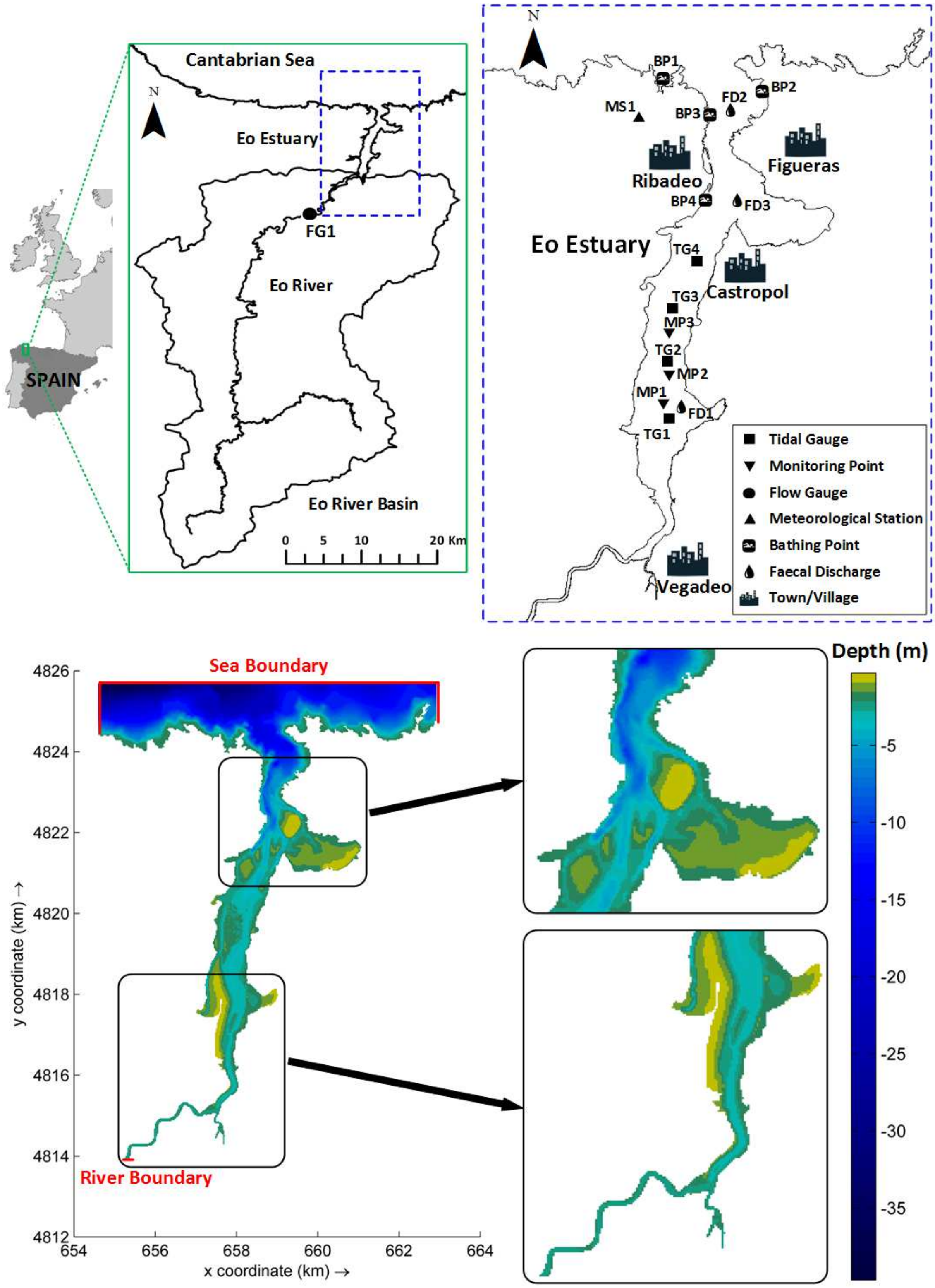

Fig. 1. Map of the Eo River Basin and the Eo Estuary, indicating the locations of the tidal gauges (TG1-TG4), monitoring points (MP1-MP3), flow gauge (FG1), meteorological station (MS1), bathing water quality control points (BP1-BP4), and faecal discharges (FD1-FD3), used in the setup of the predictive tools. Bathymetry is

also presented with a zoomed-in image of the outer and inner areas of the Eo Estuary (UTM projection ED50 30N).

At the study site, the water-related anthropic uses are recreational (e.g., swimming, sailing, and sun bathing) and economical (e.g., fishing, aquaculture, and shellfishing), and the bathing season occurs from May 1st to September 30th. Four beaches are monitored to classify their bathing quality status as regulated by Directive (2006/7/EC): Rocas Blancas (BP1), Arnao (BP2), O Cargadeiro (BP3), and Os Bloques (BP4). Due to the villages settled around the Eo Estuary, three sources of faecal pollution were discharged into the estuarine waters during the bathing seasons of 2013, 2014, and 2015 (see Fig. 1): (1) a wastewater treatment plant with biological treatment, collecting sewage from Vegadeo (FD1); (2) a submarine outfall without water treatment, collecting sewage from Castropol and Figueras (FD2); and (3) a breach in the submarine outfall in place since 2010 (FD3), constituting 24% of the FD2 flow. Dry weather conditions prevail during bathing seasons since most of the rain is received between October and April (del Río et al., 2011). Thus, storm runoff is mainly diverted to FD1 and FD2 during the bathing seasons. The other potential flowing, land-based, FIO sources (storm water discharges) are not considered in the present study as they have no flow or very low flow during bathing seasons and are not believed to affect the estuarine bathing water quality.

Regarding the available data, we retrieved information from five sources: (1) a field survey (FLTQ, 1990); (2) the Automatic Information System of the Cantabrian Hydrographic Confederation (SAI), available online at http://www.chcantabrico.es; (3) the Copernicus Marine Environment Monitoring Service (CMEMS), available online at http://marine.copernicus.eu; (4) the Meteorological Observation and Weather Forecast

Service of Galicia (MeteoGalicia), available online at www.meteogalicia.es; and (5) the Spanish Bathing Water Information System (NAYADE), available online at https://nayadeciudadano.msssi.es.

The field survey (FLTQ, 1990) took place from the 21st to the 23rd of June 1990 and included the following measurements (see Fig. 1): (1) tidal water levels at 4 points (TG1 to TG4), measured every 5 min with a tidal pressure gauge (Aanderaa WLR-5); (2) river flows, temperatures, and salinities at 1 point (FG1), measured every 2 h with an electromagnetic flow meter (Flowmate model 2000) and a limnimetric scale; (3) current speeds and directions at the bottom at 3 points (MP1 to MP3), measured every 5 min with an automatic current meter (Aanderaa RCM45); and (4) salinities and temperatures at the bottom at 3 points (MP1 to MP3), measured every 5 min with a CTD device.

From the other four sources, we retrieved data from 2013 to 2015, including (1) the daily time series of flow, salinity, and temperature at the river boundary, measured by FG1; (2) the hourly time series of salinity and temperature at the sea boundaries, modelled by the operational Iberian Biscay Irish (IBI) system of the CMEMS (Sotillo et al., 2015); (3) the hourly time series of solar radiation at the surface, recorded by MS1; and (4) the *E. coli* concentrations at the 4 monitoring stations, measured by the NAYADE (see Fig. 1): BP1 - 25 data, BP2 - 25 data, BP3 - 26 data, and BP4 - 24 data. The method for the enumeration of *E. coli* was ISO 9308-1. This method is based on membrane filtration, subsequent culture on a chromogenic coliform agar medium, and calculation of the number of target organisms in the sample.

2.2. Predictive tools

2.2.1. Process-based model

Our modelling approach was implemented in the Delft3D open-source modelling framework (http://oss.deltares.nl/web/delft3d). First, estuarine hydrodynamics were derived from the hydrodynamic module Delft3D-FLOW (Lesser et al., 2004). Second, *E. coli* concentrations were computed by means of the transport module D-Water Quality (Postma et al., 2003). This coupling has been applied in other studies, confirming its ability to simulate hydrodynamics, transport and mixing in complex aquatic systems (Los et al., 2014; Wang et al., 2016; Roberts and Villegas, 2017).

In this work, the formulation proposed by Mancini (1978) was adopted to simulate the bacterial mortality, assuming the following conditions: (1) *E. coli* was only present in the water column, without accumulating in or resuspending from sediment; (2) *E. coli* did not grow in the water column; (3) *E. coli* mortality was included as a temperature-dependent process, formulated based on first-order kinetics; and (4) the *E. coli* mortality rate was enhanced by salinity and UV radiation in an additive way. Accordingly, mortality was calculated with Eq. (1) to Eq. (5).

$$CF_{decay} = K_M \cdot C_{CF} \tag{1}$$

$$K_M = (K_B + K_{Cl}) \cdot K_T^{(T-20)} + K_R \tag{2}$$

$$K_{Cl} = k_{Cl} \cdot C_{Cl} \tag{3}$$

$$K_R = k_{rd} \cdot DL \cdot f_{uv} \cdot I_0 \frac{(1-e^{-\varepsilon H})}{\varepsilon H} \tag{4}$$

$$\varepsilon = \frac{1.8}{SD} \tag{5}$$

where CF_{decay} is the concentration of *E. coli* over time (*E. coli*/m^3·days); K_M is the first-order mortality rate (days^{-1}); C_{CF} is the *E. coli* concentration (*E. coli*/m^3); K_B is the basic mortality rate (days^{-1}); K_{Cl} is the chloride-dependent mortality rate (days^{-1}); T is the temperature (ºC); K_T is the temperature-dependent mortality rate (-); K_R is the radiation-dependent mortality rate (days^{-1}); k_{Cl} is the chloride-dependent mortality constant

(m^3/g·days); C_{Cl} is the chloride concentration (g/m^3); k_{rd} is the radiation-dependent mortality constant (m^2/W·days); DL is the day-length (days); f_{uv} is the fraction of UV light in visible light (-); I_0 is the daily solar radiation at the water surface (W/m^2); ε is the extinction of UV radiation (m^{-1}); H is the water depth (m); and SD is the Secchi disk depth (m).

2.2.2. Artificial neural networks

The basic structure of ANNs is characterized by their architecture, activation functions, and training algorithm. The ANN architecture consists of three layers (see Fig. 2): one input layer, one hidden layer that is usually composed of one layer but can be built up with more sublayers (deep learning), and one output layer (Khalil et al., 2011). Every layer has several nodes that are responsible for transmitting the information from one layer to the next layer, although neither lateral connection within any layer nor feedback connection is possible (arrows in Fig. 2).

The functioning of the ANN is as follows: Each node in the input layer supplies information to every node in the hidden layer through the "synapses". A summation of the contribution of each node in the input layer is performed in each node of the hidden layer by applying an activation function to transform the obtained value. Then, every value of every node in the hidden layer is multiplied by its weight and transmitted to the output node, where another summation is performed by applying a new activation function to obtain the final output (Wu et al., 2014).

ANNs need to be trained to assign weights accurately and, consequently, minimize errors in the output results (Motamarri and Bocelli, 2012). This task depends on the training method and the ratio of the training subset, validation subset, and test subset to the total data ($T\!:\!V\!:\!T$): the training subset is used to estimate unknown connection weights between neurons, the validation subset is used to assess the generalization ability of the trained network, and the testing subset is used to decide whether early termination is needed to avoid overfitting (Maier et al., 2010).

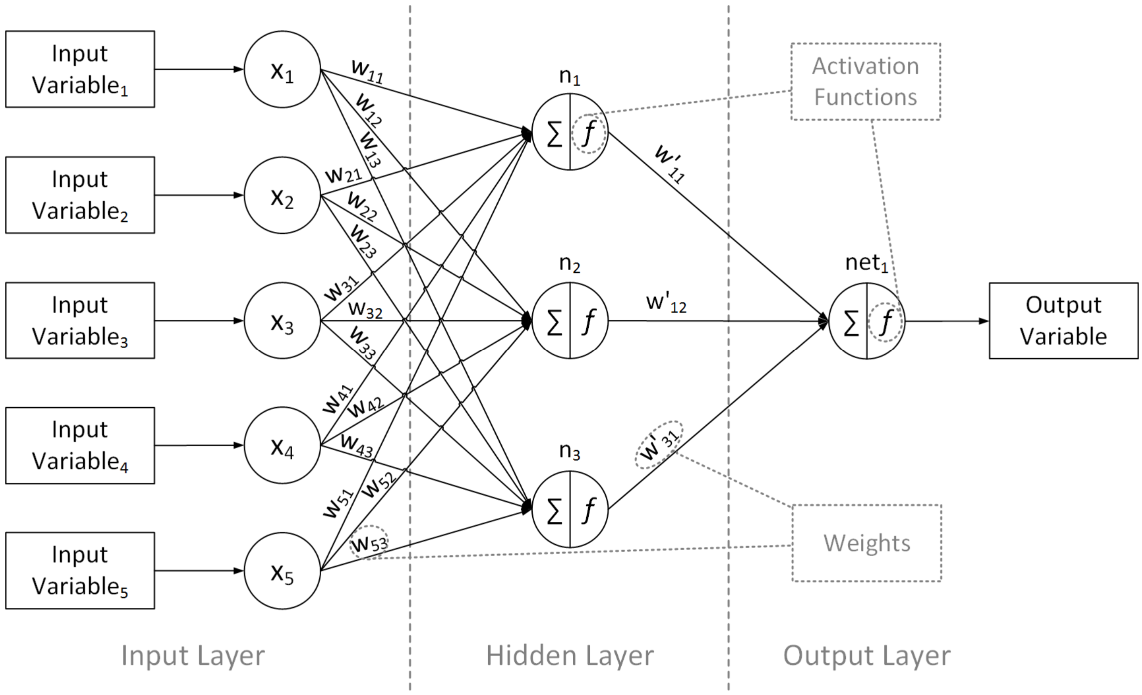

Fig. 2. Schematic view of a feedforward neural network with five nodes in the input layer, three nodes in the hidden layer and one node in the output layer. Synapses are oriented from left to right.

2.3. Performance metrics of predictive tools

2.3.1. Evaluation of predictive tools

The predictive tools' performance was evaluated by three error measurements. First, bias was calculated as the difference between the modelled results and the observed values on a given date. Second, the coefficient of determination (R^2) was determined as expressed in Eq. (6).

$$R^2 = \frac{\sum_{i=1}^{N}(S_i - \bar{R}_i)^2}{\sum_{i=1}^{N}(R_i - \bar{R}_i)^2} \quad (6)$$

where R_i is the i-field data of the measurements, S_i is the i-model data of the simulations (process-based or ANN), $\bar{R}$ is the average of the measurements, and i is the i^{th} value from 1 to N measurements (laboratory analyses).

Third, the error between the series was calculated using the model efficiency (CE), developed by Nash and Sutcliffe (1970), as displayed in Eq. (7).

$$CE = 1 - \frac{\sum_{i=1}^{N}(R_i - S_i)^2}{\sum_{i=1}^{N}(R_i - \bar{R})^2} \quad (7)$$

The CE ranges between -∞ and 1.0 (1.0 inclusive), with CE=1 being the optimal value. Values between 0.0 and 1.0 are generally viewed as acceptable levels of performance, whereas values <0.0 indicate that the mean observed value is a better predictor than the simulated value, which indicates unacceptable performance. Depending on the CE value, the comparison is considered acceptable (poor) if CE<0.4, acceptable (-) if 0.4≤CE<0.6, acceptable (convenient or good) if 0.6≤CE<0.8, and acceptable (excellent) if CE≥0.8.

2.3.2. Accuracy of predictive tools for bathing water quality management

The contingency table (Table 1a) and its error metrics (Table 1b) were employed to assess the accuracy of predictive tools in predicting the compliance with and/or exceedance of the FIO concentrations at specific thresholds (Manzato, 2007; Bennett et al., 2013; Bedri et al. 2016). Contingency tables establish the number of occurrences where predictive tools have generated correct predictions (see Table 1a): (1) the exceedance of specific values (hits); (2) the occurrences of correct negatives; (3) the number of alarms missed by the model; and (4) the number of false alarms. Therefore, an ideal model would have data in only the hits and correct negatives categories. Table 1b lists the error metrics of the contingency table used in the current study along with their limits and ideal values.

		Observed Exceedances		
		yes	no	
Predicted Exceedances	yes	Hits	False alarms	Predicted yes
	no	Misses	Correct negatives	Predicted no
		Observed yes	Observed no	Total

a) Contingency table

Metric	Formula	Range of values	Ideal value	Notes
Accuracy (fraction correct)	$\frac{Hits + Correct\ negatives}{Total}$	0-1	1	It is heavily influenced by the most common category, usually "no event".
Bias score (frequency bias)	$\frac{Hits + False\ alarms}{Hits + Misses}$	0-∞	1	Indicates if the model tends to under- (<1) or over- (>1) estimate.
Hit rate (Probability of detection)	$\frac{Hits}{Hits + Misses}$	0-1	1	Sensitive to hits but ignores false alarms. Good for rare events.
False alarm rate (Probability of false detection)	$\frac{False\ alarms}{False\ alarms + Correct\ negatives}$	0-1	0	Sensitive to false alarms but ignores misses.
Success index	$\frac{1}{2} \cdot \left[\frac{Hits}{Hits + Misses} + \frac{Correct\ negatives}{Total}\right]$	0-1	1	Weights equally the ability of the model to correctly detect occurrences and non-occurrences of events.
Threat score	$\frac{Hits + Correct\ negatives}{Total}$	0-1	1	Measures the fraction of observed cases that were correctly modelled. It penalizes both misses and false alarms.

b) Error metrics

Table 1. (a): Contingency table to assess the accuracy of predictive tools for the prediction of faecal indicator organism (FIO) concentrations. (b): Error metrics of the contingency table (Source: Manzato, 2007; Bennett et al., 2013; Bedri et al. 2016).

2.4. Methodology to develop artificial neural networks for the analysis of bathing water quality in estuaries

The overall approach, illustrated in Fig. 3, integrates a coupled hydrodynamic-bacteriological model previously calibrated with field data at the bathing sites into a real-time framework by using ANNs trained on the numerical model outputs (targets).

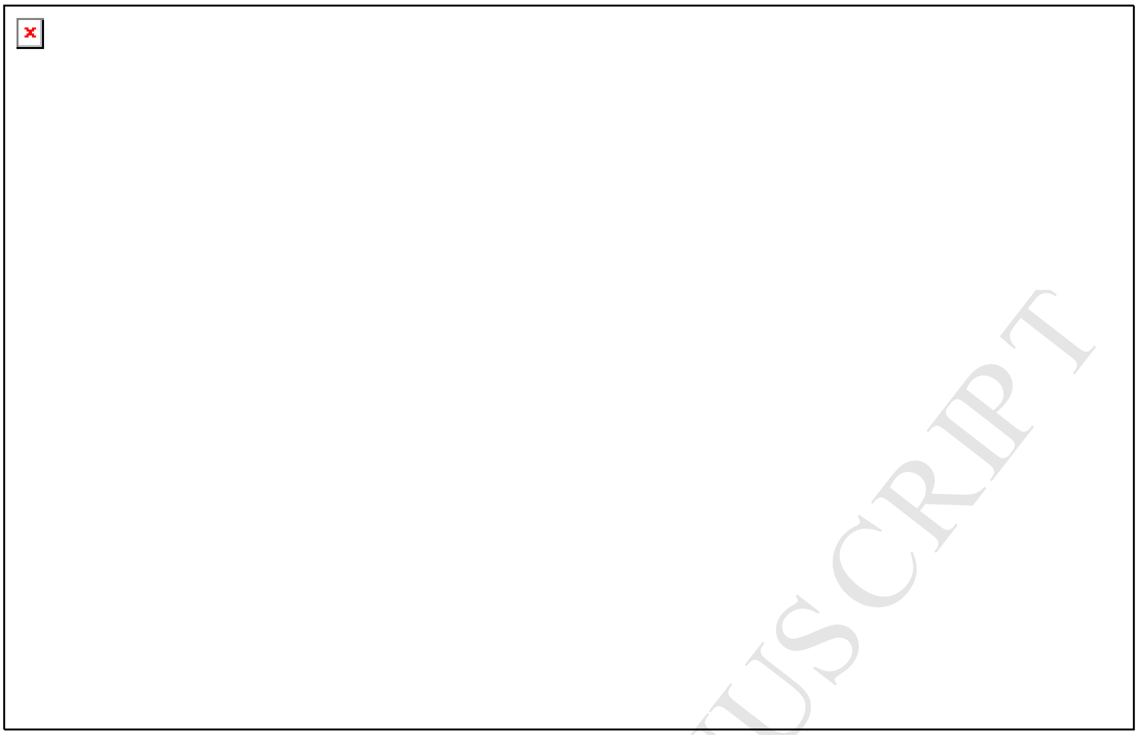

Fig. 3. Overall methodological approach.

Since critical decisions must be made when developing an ANN, we use a five-step method (see Fig. 4).

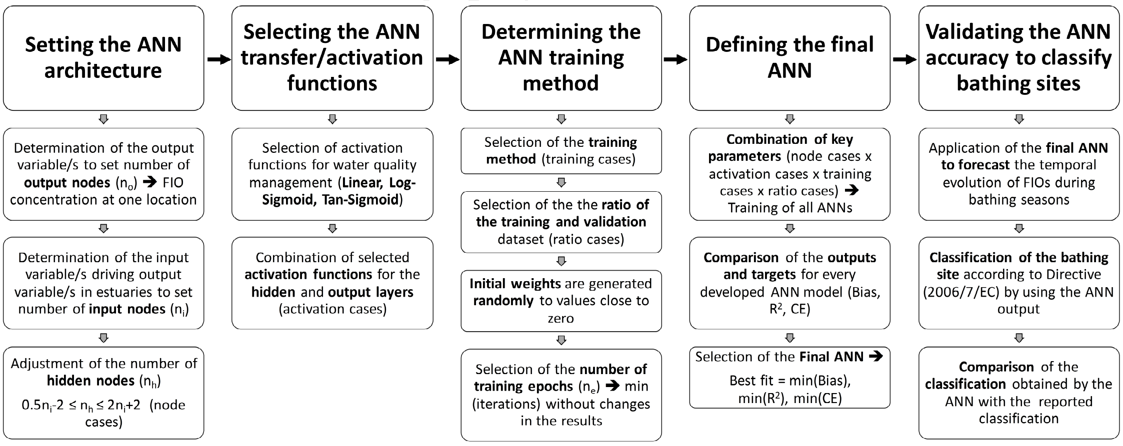

Fig. 4. Schematic view of the proposed methodology to develop artificial neural networks to analyse bathing water quality criteria in estuaries.

2.4.1. Setting the ANN architecture

Since the ANN output is the evolution of FIO concentration at one bathing site, the number of nodes in the output (n_o) is one.

Bearing in mind that ANN models will be emulators of process-based models, ANN inputs should be process-based model inputs, i.e., boundary conditions, sinks and sources. Thus, the input variables are hydrodynamic forcings, water constituents at open boundaries, atmospheric forcings, and faecal discharges, and the number of nodes in the input (n_i) should therefore be determined from this preliminary selection based on site-specific conditions.

The number of nodes in the hidden layer (n_h) should be less than twice n_i (Motamarri and Bocelli, 2012); we propose Eq. (8) to set n_h.

$$0.5 \cdot n_i - 2 \leq n_h \leq 2 \cdot n_i + 2 \tag{8}$$

2.4.2. Selecting the ANN transfer/activation functions

Three different activation functions are widely used (Jiang et al., 2013) for the transfer between the input and hidden layer (f_h) and the hidden and output layers (f_o): (1) the linear transfer function (Eq. (9)); (2) the log-sigmoid transfer function (Eq. (10)); and (3) the tan-sigmoid transfer function (Eq. (11)). Generally, sigmoid functions are used for pattern recognition, whereas linear functions are used for fitting.

$$f(x) = x \tag{9}$$

$$g(x) = \frac{1}{1+e^{-x}} \tag{10}$$

$$h(x) = \frac{2}{1+e^{-2x}} - 1 \tag{11}$$

2.4.3. Determining the ANN training method

Several methods are used for training ANNs, with the Levenberg-Marquardt method (Hagan and Menhaj, 1994) and the backpropagation algorithm (Rumelhart et al., 1986) being the most common. Additionally, the initial weights are generated randomly to obtain values close to zero, and the $T{:}V{:}T$ ratio should be adjusted by trial and error

(Wu et al., 2014). Lastly, the number of training epochs (n_e) is decided based on trials by observing the conditions under which ANN training and testing results are both independent of the number of iterations (Tufail et al., 2008).

2.4.4. Defining the final ANN

The key parameters are combined to develop several ANN models (n_h, f_h, f_o, training methods, and $T{:}V{:}T$). Next, these models are trained, and the ANN model displaying the lowest error metric between outputs and targets (final ANN) is chosen (Zou et al., 2007).

2.4.5. Validating the ANN accuracy to classify bathing sites

The final ANN model is applied to forecast FIO concentrations at the bathing site during bathing seasons. Next, the ANN results are classified according to the standard values set in Directive (2006/7/EC) and compared with the official reported classification.

2.5. Setup of predictive tools in the Eo Estuary

2.5.1. Setup of the process-based model

The Eo Estuary was represented horizontally using a 3D rectangular mesh grid composed of 332x640 grid cells with a horizontal resolution of 25x25 m^2, 3 vertical σ-layers equally spaced along the water column, and the bathymetry displayed in Fig. 1. The hydrodynamic calibration was performed for the period between the 21st and 24th of June 1990, including a spin-up period of 30 days to allow the hydrodynamic and thermohaline variables to interact and adjust themselves. Once the hydrodynamic module was calibrated, the hydrodynamics of the 2013, 2014, and 2015 bathing seasons driven by the tidal action and river flows (see Fig. S1 in the supplementary materials) were simulated as required inputs for the water quality module calibration. For a more detailed description of the hydrodynamic module setup, readers are referred to the supplementary materials.

Next, we implement the transport module in the same grid, the same time step (6 s), the same four open boundaries (see Fig. 1), and the same spin-up period of 30 days used in the hydrodynamic module setup (see the supplementary materials). The initial condition was 0 *E. coli*/100 ml in the whole model domain. Based on the available data at the sea and river boundaries, the mean concentration of these measurements was used as a constant boundary condition, with 0 and 850 *E. coli*/100 ml at the sea and river boundaries, respectively. Table 2 lists the parameters used in the calculation of the *E. coli* transport and mixing in the Eo Estuary.

Constant	Value	Units	Source
D_H, D_V	Time series	m^2/s	Hydrodynamic module
T	Time series	ºC	Hydrodynamic module
C_{Cl}	Time series	g/m^3	Hydrodynamic module
I_0	Time series	W/m^2	Meteorological station (MS1)
K_B	0.8	1/days	Chapra (1997)
DL	1	days	(*)
f_{uv}	0.12	-	Diffey (2002)
ε	0.35	1/m	FLTQ (1990); Eq. (5)
K_T	1.07	-	This study (calibration)
k_{rd}	0.086	$m^2/W\cdot days$	This study (calibration)
k_{Cl}	$2\cdot 10^{-4}$	$m^3/g\cdot days$	This study (calibration)

(*) Day-night variations are considered within the irradiation (I_0).

Table 2. Model parameters used in the calculation of *E. coli* transport and mixing.

Based on the data from Metcalf and Eddy, Inc. (2003) for a single day, the hourly flow of three faecal discharges (FD1-FD3) was introduced (see Fig. S2 in the supplementary materials). The mean discharge flow (in m^3/s) was 0.00347, 0.00524 and 0.00165 for FD1, FD2 and FD3, respectively. The constant discharge concentration (in *E. coli*/100 ml) was 10^6, 10^8 and 10^8 for FD1, FD2 and FD3, respectively. Finally, a constant salinity and temperature of 0 psu and 17 ºC, respectively, were specified for the three discharges.

2.5.2. Setup of the artificial neural network

ANNs were developed for BP1, BP2, BP3, and BP4. First, the output variable was the *E. coli* concentration at every bathing site; thus, n_o was set to one for every ANN. n_i was fixed by the process-based model inputs, with a value of 9 in the Eo Estuary: water level, salinity and temperature at the sea boundary; flow and temperature at the river boundary; solar radiation; and the flow of the three faecal discharges (FD1-FD3). Note that the model inputs obtained with constant values were not included as input variables in the ANN models, i.e., salinity at the river boundary (see the supplementary materials) and salinity, temperature and *E. coli* concentrations of faecal discharges (see subsection 2.5.1). Following Eq. (8), 3, 7, 11, 15, or 19 n_h were selected (5 node cases). Second, we combined the 3 activation functions, obtaining 9 activation cases. Third, 9 training methods were tested: BFGS quasi-Newton backpropagation, resilient backpropagation, scaled conjugate gradient backpropagation, conjugate gradient backpropagation with Powell-Beale restarts, Levenberg-Marquardt backpropagation, conjugate gradient backpropagation with Fletcher-Reeves updates, conjugate gradient backpropagation with Polak-Ribiére updates, one step secant backpropagation, and gradient descent with momentum and adaptive learning rate backpropagation. Fourth, 3 $T{:}V{:}T$ ratios were defined: 60:20:20, 70:15:15, and 80:10:10. Finally, the initial weights used were generated randomly to obtain values close to zero, and n_i was set to 10^3 for all ANN models, based on previous trials.

For every bathing site, the combination of 5 node cases, 9 activation cases, 9 training cases, and 3 ratio cases resulted in 1215 ANN models. These models were trained, validated and tested using the hourly evolution of *E. coli* concentration computed by the process-based model during the bathing seasons of 2013, 2014, and 2015 as targets (11019 modelled concentration measurements). Next, outputs and targets were compared by means of bias, CE, and R^2. The best fits (final ANNs) were obtained with 15 n_h, a tan-sigmoid function for the f_h, a log-sigmoid function for the f_o, a Levenberg-Marquardt backpropagation method, and a $T:V:T$ ratio of 70:15:15.

3. Results

3.1. Hydrodynamics

The results provided by the hydrodynamic module were compared with the available measurements. For water levels, the bias ranged between -0.04 and 0.10 m, and the CE ranged between 0.98 and 0.99 (see Fig. S3 in the supplementary materials). For current velocities, the bias ranged between 0.01 and 0.02 m/s, and the CE ranged between 0.87 and 0.91 (see the left panels of Fig. S4 in the supplementary materials). For salinities, the bias ranged between -0.39 and -0.29 psu, and the CE ranged between 0.92 and 0.98 (see the right panels of Fig. S4 in the supplementary materials). Overall, these errors confirmed that the hydrodynamic module satisfactorily reproduced water circulation and transport throughout the Eo Estuary.

3.2. Predictive tools

3.2.1. Evaluation of predictive tools

Fig. 5 shows scatter density plots for the *E. coli* concentrations between the outputs provided by each final ANN model and the targets simulated by the process-based model at BP1 (a), BP2 (b), BP3 (c), and BP4 (d) for the bathing seasons of 2013, 2014, and 2015. The colorbar of Fig. 5 displays the occurrence probability of the scatter dots defined by the *E. coli* concentration of targets (process-based model) and outputs (ANN model).

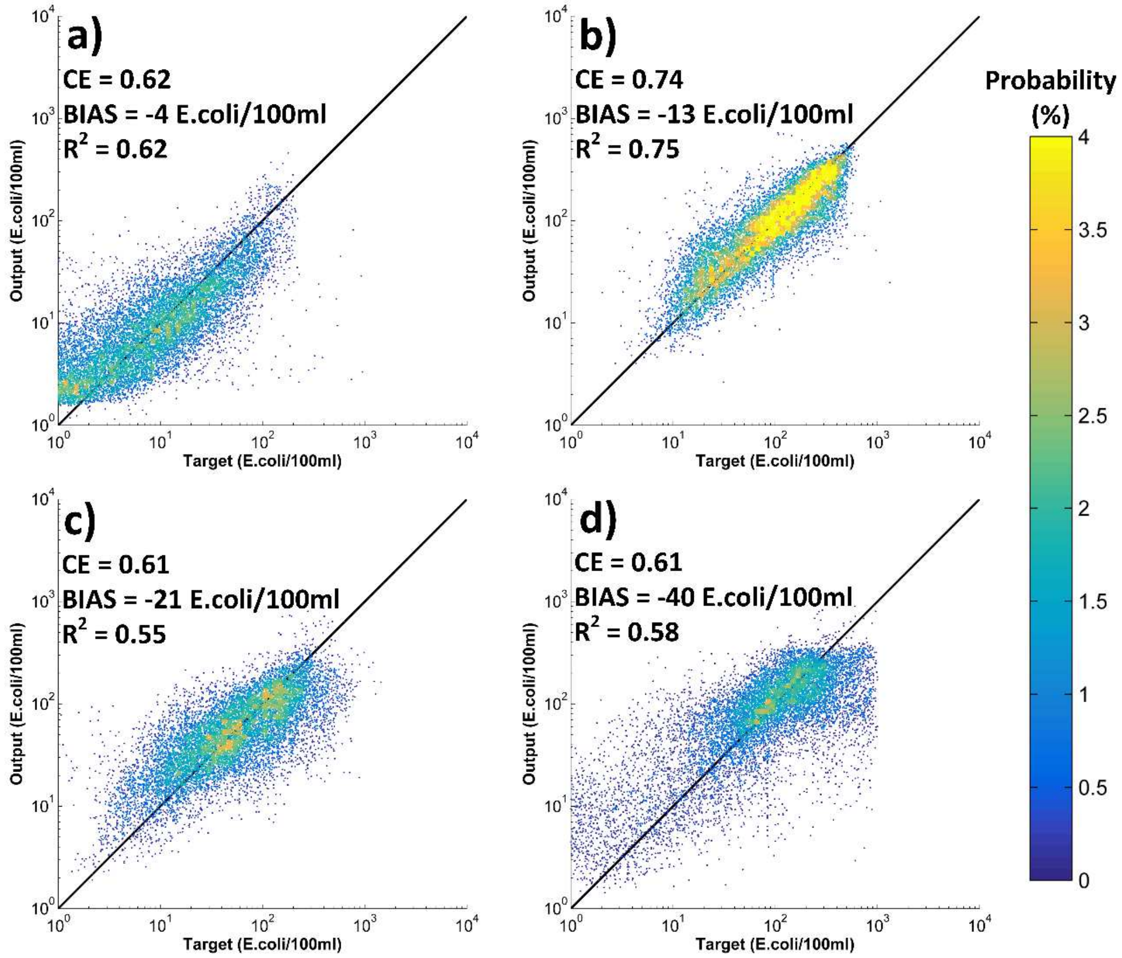

Fig. 5. Performance of the final artificial neural networks (outputs) in emulating *E. coli* concentrations (*E. coli*/100 ml) computed by the process-based model (targets) at BP1 (a), BP2 (b), BP3 (c), and BP4 (d). The bias, R^2, and CE magnitudes are also shown for the four bathing sites (BP1-BP4). The colorbar shows the occurrence probability of the scatter dots defined by the *E. coli* concentration of targets (process-based model) and outputs (ANN model).

In the four ANNs, the bias ranged between -4 and -40 *E. coli*/100 ml (the minus sign indicates that the output concentrations were smaller than the target concentrations), the

R^2 ranged between 0.55 and 0.75, and the CE ranged between 0.61 and 0.74. These error metrics confirmed that the four ANN models efficiently detected and calculated the temporal evolution of *E. coli* concentrations, preserving the accuracy of the results. A detailed examination by location revealed that the best performance (yellow to green dots in Fig. 5) was obtained at BP2, followed by BP1, BP4, and BP3.

Next, the results provided by the process-based model and the final ANNs were compared with the available measurements at the four bathing sites during the bathing seasons of 2013, 2014, and 2015 (see Figs. S5, S6, and S7 in the supplementary materials, respectively). Fig. 6 shows the performance of the process-based (filled markers) and ANN (unfilled markers) models in simulating *E. coli* concentrations at BP1 (squares), BP2 (circles), BP3 (diamonds), and BP4 (triangles) during the bathing season of 2013 (red), 2014 (green), and 2015 (blue).

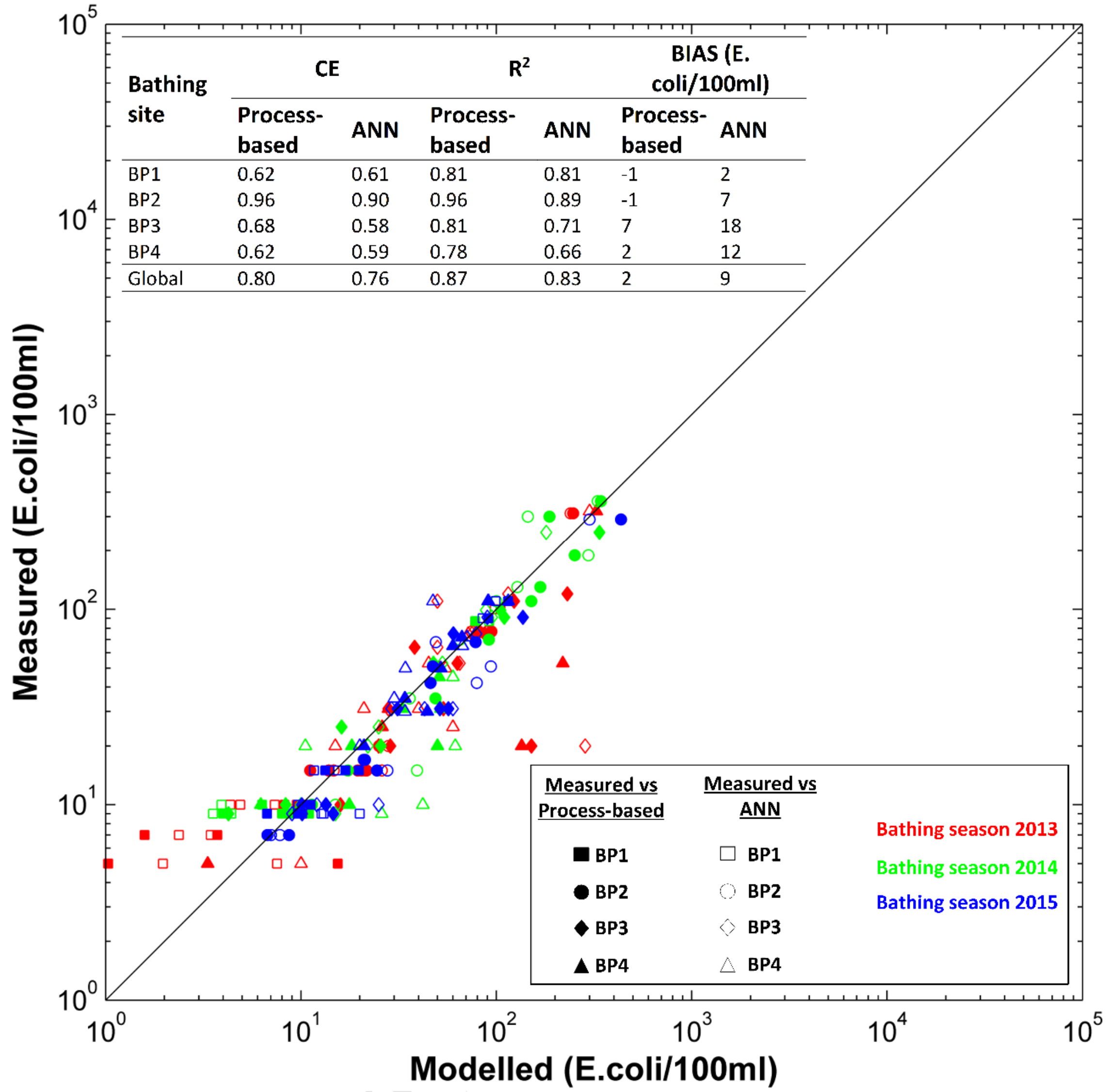

Bathing site	CE		R^2		BIAS (E. coli/100ml)	
	Process-based	ANN	Process-based	ANN	Process-based	ANN
BP1	0.62	0.61	0.81	0.81	-1	2
BP2	0.96	0.90	0.96	0.89	-1	7
BP3	0.68	0.58	0.81	0.71	7	18
BP4	0.62	0.59	0.78	0.66	2	12
Global	0.80	0.76	0.87	0.83	2	9

Fig. 6. Performance of the process-based model (filled markers) and the ANN models (unfilled markers) in simulating *E. coli* concentrations (*E. coli*/100 ml) at BP1 (squares), BP2 (circles), BP3 (diamonds), and BP4 (triangles) during the bathing season of 2013 (red), 2014 (green), and 2015 (blue). The bias, R^2, and CE magnitudes are also shown for the four bathing sites (BP1-BP4) and considering all the bathing seasons and locations at the same time (global).

As displayed in Fig. 6, the global bias, R^2, and CE were 2 and 9 *E. coli*/100 ml, 0.87 and 0.83, and 0.80 and 0.76 for the process-based model and the ANN model, respectively.

These metrics indicate a slightly better fit for the process-based model. Moreover, Fig. 6 summarizes the performance of both predictive tools at the four bathing sites. The results showed that the *E. coli* concentrations at BP2 were excellently (CE>0.8) predicted by both tools (R^2>0.89). In the case of BP1, predictions were good (CE>0.6) for both tools (R^2=0.81), and at BP3 and BP4, the *E. coli* concentrations were conveniently (CE>0.6) predicted by the process-based model (R^2>0.78) and acceptably (CE>0.4) predicted by the ANN model (R^2>0.66). Therefore, these error metrics confirm that the process-based model and the ANN model satisfactorily reproduced the evolution of *E. coli* concentrations throughout the Eo Estuary, indicating the ability of both predictive tools to model the mortality, transport and mixing of *E. coli*.

3.2.2. Accuracy of predictive tools for bathing water quality management

The results provided by laboratory analyses, process-based models or ANN models led to a bathing water classification of “excellent quality” at the 4 bathing sites (95th percentile < 250 *E. coli*/100 ml). Moreover, the 95th percentile values of the datasets for the laboratory analyses, the process-based model, and the ANN model were 98, 97, and 102 *E. coli*/100 ml at BP1; 232, 245, and 249 *E. coli*/100 ml at BP2; 118, 164, and 211 *E. coli*/100 ml at BP3; and 110, 109, and 206 *E. coli*/100 ml at BP4, respectively.

Table 3 lists the calculated error metrics of the contingency table to assess the accuracy of the predictive tools in predicting the compliance with or exceedance of *E. coli* concentrations of 500, 250, 125, 50, and 25 *E. coli*/100 ml.

Bathing site	**Contingency table (metrics)**	**Value = 500 *E. coli*/100 ml**		**Value = 250 *E. coli*/100 ml**		**Value = 125 *E. coli*/100 ml**		**Value = 50 *E. coli*/100 ml**		**Value = 25 *E. coli*/100 ml**	
		Process-based	**ANN**	**Process-based**	**ANN**	**Process-based**	**ANN**	**Process-based**	**ANN**	**Process-based**	**ANN**
BP1	Accuracy	1.00	1.00	1.00	1.00	1.00	1.00	1.00	1.00	1.00	1.00
	Bias score	(*)	(*)	(*)	(*)	(*)	(*)	1.00	1.00	1.00	1.00
	Hit rate	(*)	(*)	(*)	(*)	(*)	(*)	1.00	1.00	1.00	1.00
	False alarm rate	0.00	0.00	0.00	0.00	0.00	0.00	0.00	0.00	0.00	0.00
	Success index	(*)	(*)	(*)	(*)	(*)	(*)	0.92	0.92	0.92	0.92

	Threat score	(*)	(*)	1.00	1.00	1.00	1.00	1.00	1.00	1.00	1.00
BP2	Accuracy	1.00	1.00	0.88	0.88	0.96	1.00	0.96	0.92	0.96	0.84
	Bias score	(*)	(*)	1.33	1.33	0.86	1.00	1.09	1.00	0.93	0.78
	Hit rate	(*)	(*)	0.67	0.67	0.86	1.00	1.00	0.92	0.93	0.78
	False alarm rate	0.00	0.00	0.09	0.09	0.00	0.00	0.07	0.08	0.00	0.00
	Success index	(*)	(*)	0.73	0.73	0.79	0.88	0.76	0.70	0.67	0.53
	Threat score	(*)	(*)	0.88	0.88	0.96	1.00	0.96	0.92	0.96	0.84
BP3	Accuracy	1.00	1.00	0.96	0.96	0.88	0.96	0.77	0.92	0.88	0.96
	Bias score	(*)	(*)	0.00	0.00	0.25	0.50	0.85	0.82	0.83	0.94
	Hit rate	(*)	(*)	0.00	0.00	0.25	0.50	0.69	0.82	0.83	0.94
	False alarm rate	0.00	0.00	0.00	0.00	0.00	0.00	0.15	0.00	0.00	0.00
	Success index	(*)	(*)	0.48	0.48	0.55	0.71	0.56	0.68	0.56	0.62
	Threat score	(*)	(*)	0.96	0.96	0.88	0.96	0.77	0.92	0.88	0.96
BP4	Accuracy	1.00	1.00	1.00	1.00	0.92	1.00	0.90	0.73	0.91	0.83
	Bias score	(*)	(*)	1.00	1.00	0.33	1.00	0.78	0.78	0.88	0.88
	Hit rate	(*)	(*)	1.00	1.00	0.33	1.00	0.78	0.56	0.88	0.82
	False alarm rate	0.00	0.00	0.00	0.00	0.00	0.00	0.00	0.15	0.00	0.17
	Success index	(*)	(*)	0.98	0.98	0.60	0.98	0.67	0.53	0.57	0.52
	Threat score	(*)	(*)	1.00	1.00	0.92	1.00	0.90	0.73	0.91	0.83

(*) Indeterminate form 0/0.

Table 3. Computed metrics for the assessment of the accuracy of the predictive tools in predicting compliance with/exceedance of the *E. coli* values of 500, 250, 125, 50, and 25 *E. coli*/100 ml.

Regardless of the metric in Table 3 used, the predictive tools presented the following pattern of performance: (1) the performances of the predictive tools for any concentration value was the same at BP1, with a success index of 0.92; (2) the predictive tools exhibited the same performance for the values of 500 and 250 *E. coli*/100 ml, with a success index for the value of 250 *E.coli*/100 ml of 0.73, 0.48, and 0.98 at BP2, BP3, and BP4, respectively; (3) the ANN models performed better than the process-based model for the value of 125 *E. coli*/100 ml, with a success index of the process-based and ANN models of 0.79-0.88, 0.55-0.0.71, and 0.60-0.98 at BP2, BP3, and BP4, respectively; and (4) the process-based model performed better than the ANN models for low values (50 and 25 *E. coli*/100 ml) at BP2 and BP4 and worse than these models for low values at BP3. For instance, the success index of the process-based and the ANN models for the value of 50 *E. coli*/100 ml was 0.76-0.70, 0.56-0.68, and 0.67-

0.53 at BP2, BP3, and BP4, respectively. Overall, these metrics indicated that the process-based and ANN models satisfactorily predicted the compliance with/exceedance of *E. coli* concentrations of 500, 250, 125, 50, and 25 *E. coli*/100 ml and, hence, adequately classified the bathing sites located in the Eo Estuary.

3.3. Configuration and computational trade-off of artificial neural networks

The final ANN configuration was obtained with 15 n_h, a tan-sigmoid function for the f_h, a log-sigmoid function for the f_o, a Levenberg-Marquardt backpropagation method, and a $T\!:\!V\!:\!T$ ratio of 70:15:15. Table 4 summarizes the configuration of ANN models developed in other studies, including the predicted FIO, n_i, n_h, f_h, f_o, training method, n_e, $T\!:\!V\!:\!T$, and R^2.

Study	FIO(*)	n_i	n_h	f_h(**)	f_o(**)	Training method	n_e	$T\!:\!V\!:\!T$	R^2
Chandramouli et al. (2007)	FC	7	9	Log	Log	Back-propagation	(***)	75:15:10	0.63-0.94
Mas and Ahlfeld (2007)	FC	6	16	Tan	Tan	Levenberg-Marquardt	10^3	64:16:20	(***)
Kim et al. (2008)	EC	3	1	Tan	Tan	Back-propagation	$5\cdot10^4$	72:8:20	0.90-0.96
He and He (2008)	TC	7	3	(***)	(***)	Back-propagation	(***)	56:24:20	0.79
He and He (2008)	FC	12	6	(***)	(***)	Back-propagation	(***)	56:24:20	0.82
He and He (2008)	EN	7	8	(***)	(***)	Back-propagation	(***)	56:24:20	0.86
Tufail et al. (2008)	EC	2	4	Log	Log	Back-propagation	10^4	80:20:(***)	0.58-0.73
Kazemi Yazdi and Scholz (2010)	EN	4	8	Tan	Tan	Levenberg-Marquardt	10^3	65:15:20	0.15-0.80
Keeratipibul et al. (2011)	EC	6	5	Tan	Log	Back-propagation	(***)	70:30:(***)	0.72
Thoe et al. (2012)	FC	7	5	Log	Lin	Gradient descent with momentum	10^3	60:20:20	0.29-0.75
Motamarri and Boccelli, (2012)	FC	5	6	Tan	Lin	Levenberg-Marquardt	10^3	99:1 (leave-one-out)	(***)
Thoe et al. (2014)	FC	12	5	Log	Lin	Gradient-descent	$2\cdot10^4$	60:20:20	0.38-0.58
Zhang et al. (2015)	FC	14	(***)	(***)	(***)	Back-propagation	(***)	60:20:20	0.68
This study (2018)	EC	9	15	Tan	Log	Levenberg-Marquardt	10^3	70:15:15	0.55-0.75

(*) FC: *Faecal coliform*, TC: *Total coliform*, EC: *E. coli*, EN: *Intestinal enterococci*.
(**) Log: Log-sigmoid, Tan: Tan-sigmoid, Lin: Linear.
(***) Non-specified in the study.

Table 4. Review of previous research predicting faecal indicator organisms (FIOs) with multilayer feedforward networks consisting of one input layer, one hidden layer, and one output layer.

As displayed in Table 4, ANN models were applied to predict FC (50%), EC (29%), EN (14%), and TC (7%) concentrations. The ratio between n_h and n_i (n_h: n_i) ranged from 0.33 to 2.66, with a mean value of 1.17. For f_h, the log-sigmoid, tan-sigmoid and linear functions were used 4, 6, and 0 times, respectively. In the case of f_o, these functions were used 4, 3, and 3 times, respectively. Back-propagation was the most commonly used training method (56%), followed by the Levenberg-Marquardt (28%) and gradient descent methods (16%). n_e ranged between 10^3 and $5{\cdot}10^4$, with the most commonly used value being 10^3 (72%). Regarding T: V: T, the studies considered a range of the total data available from 56% to 80% for training, from 1% to 30% for validation, and from 0% to 20% for testing. Based on these ratios, the mean value of T: V: T was 67:18:15. Finally, the R^2 varied between 0.15 and 0.94, with a mean value of 0.68.

All simulations were executed on a desktop machine with an Intel Core i7-3770 3.4 GHz, 64-bit, and 16 GB RAM. Fig. 7 displays the computational times to simulate *E. coli* concentrations by the process-based and ANN approaches. In Fig. 7, note that Forecasting: 1 h, Forecasting: 1 day, Forecasting: 1 month, and Forecasting: 1 bathing season refer to the simulation times.

The process-based model calibration was the first step for both approaches, requiring 336 and 168 h for the calibration of hydrodynamics and water quality modules, respectively. The second step was applied only in the ANN approach, requiring 144 h for the development of ANN models. At this step, both approaches were ready to forecast FIO concentrations, with computational times (in hours) of the process-based and ANN models for 1 h, 1 day, 1 month and 1 bathing season of 0.25 and 0.01, 6 and 0.01, 78 and 0.02, and 0.03 and 949, respectively.

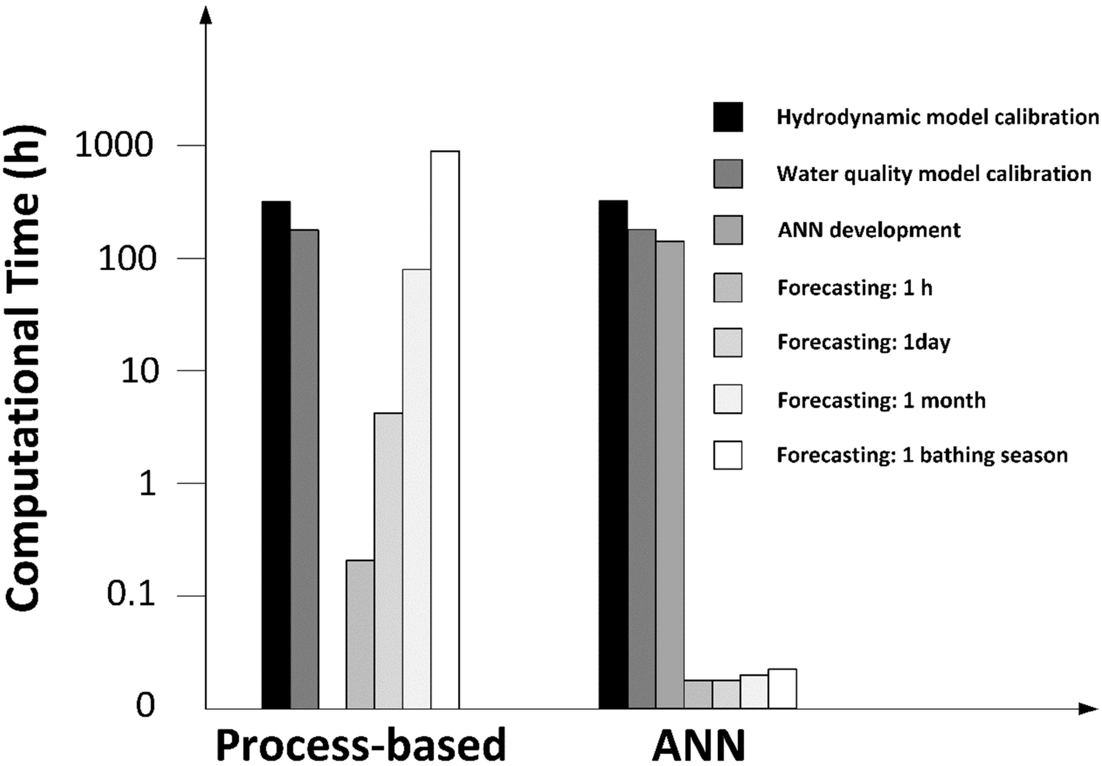

Fig. 7. Computational times used to simulate FIO concentrations by the process-based model and by the ANN model using the proposed methodology. Note that Forecasting: 1 h, Forecasting: 1 day, Forecasting: 1 month, and Forecasting: 1 bathing season refer to the simulation times.

4. Discussion

4.1. Performance of predictive tools

While the results indicate that *E. coli* prediction using the process-based model throughout the Eo Estuary is reasonably accurate, inconsistencies between measured and predicted *E. coli* concentrations may still occur because the required numerical precision is subject to the uncertainties in FIO enumeration methods, the complicated relationships and processes related to FIO evolution, the impact of the changing environment on FIO concentrations, and/or the model accuracy limits (Boehm, 2007; Gronewold and Wolpert, 2008; Shaw et al. 2017).

Since the ANN models were trained by means of the process-based model outputs, their predictions were slightly worse because they were also biased by the process-based model errors (see Fig. 6). In this regard, the ANN models mostly underestimated/overestimated *E. coli* concentrations compared with the process-based model for magnitudes higher/lower than a specific value because the neural network approach smoothed the results provided by the process-based model (see Figs. S5 to S7 in the supplementary materials). For instance, *E. coli* concentrations were underestimated/overestimated for magnitudes higher/lower than 20, 80, 50, and 90 *E. coli*/100 ml at BP1, BP2, BP3, and BP4, respectively (see Fig. 5). This effect was generated by the kernel of the network consisting of nonlinear relationships that prioritized larger weights for the values with a higher frequency of input data because the networks were designed to minimize statistical errors.

Moreover, predictions were better in BP2 than in BP1, BP3 and BP4 because this beach is the most influenced by hydrodynamics, i.e., advection processes were more significant than diffusion and reaction processes. The factors that may influence these differences are the discharge locations and beach locations related to the main estuarine water inflows and outflows. The three discharges are located in the main channel close to the eastern margin, such that faecal pollution is transported by the main estuarine water flows along the main channel until it reaches the adjacent coastal area (advection). Thus, *E. coli* levels presented higher values with less variability at the main channel and were higher at the eastern margin than at the western margin. In other estuarine areas such as tidal flats or the western margin, diffusion processes become significant for transporting faecal pollution due to lateral dispersion with respect to the main flow direction; as a result, the *E. coli* levels presented lower values with more variability. Lastly, the coastal areas outside the estuary displayed the lowest *E. coli* concentrations because the reaction processes are significant in the transport of faecal pollution due to the greater distance to the discharge locations, which increases the travel time and, subsequently, the bacterial mortality.

First, BP2 is located in the main channel at the eastern margin and close to FD2 (the major faecal discharge in the estuary). Due to the location of this point, the evolution of *E. coli* concentrations presented higher values with less variability than that at BP1, BP3 and BP4, increasing the accuracy of both predictive tools. Second, BP3 and BP4 are located outside the main channel at the western margin and close to FD2 and FD3, respectively. Due to the locations of these points, the evolution of *E. coli* concentrations presented lower values with more variability than that at BP2, decreasing the accuracy of both predictive tools. Finally, BP1 is located at the adjacent western coastal area, outside the estuary. Due to the location of this point, the evolution of *E. coli* concentrations presented the lowest values and less variability than that at BP3 and BP4 and more than that at BP2, leading to a better accuracy of both predictive tools at this point than at BP3 and BP4 and a worse accuracy than at BP2.

One way to minimize the impact of imprecise and variable data quality is to categorize data into overlapping groups and frequencies that have meaning relative to the system under study rather than focusing on predicting a specific concentration (Chandramouli et al., 2007). Thus, we used a contingency table as an error metric to calculate the accuracy of predictive tools for bathing water quality management. For the *E. coli* value of 500 at BP1, BP2, BP3 and BP4, the performance of both predictive tools was the same because this performance is heavily influenced by the most common category, namely, “correct negative” (see Table 1), due to the concentration measurements always being below this threshold. This performance was also observed at BP1 for the *E. coli* values of 250 and 125. The ANN models performed better than the process-based model for intermediate values and worse for low values because the neural network approach smoothed the results.

Efforts are currently underway to expand this methodology to include a neural network approach using deep learning (Schmidhuber, 2015), considering the real-time flow, salinity, temperature and *E. coli* concentration of faecal discharges (Bravo et al., 2017), including the effect of other forcings such as wind and/or waves (Dunn et al., 2014), and taking into account the effect of extreme events such as those produced after heavy rain or due to a failure in the sewer system.

4.2. Configuration and computational trade-off of artificial neural networks

The application of ANNs to the Eo Estuary presented here was in accordance with the ANN configurations proposed in other studies. Our final ANN configuration confirmed the tendency to develop ANN models with an $n_h\!:n_i$ ratio higher than 1 and the validity of the proposed Eq. (8) as an indicator of the suitable range for trials with n_h. Moreover, our review suggests that the best configuration for predicting FIOs with ANNs might be structured with a $1<n_h\!:n_i<2$ ratio, a tan-sigmoid function for the f_h, a log-sigmoid function for the f_o, the Levenberg-Marquardt method, a 10^3 n_e, and a $T\!:V\!:T$ ratio of 67:18:15. However, it should be emphasized that there is not a predefined ANN configuration that ensures the best approximation of the outputs for the targets.

Although ANN models need to be trained and validated, which is a time-consuming process, one of the most valuable characteristics of ANNs is their ability to perform long-term forecasting with computational times that barely exceed one minute. For instance, this study highlighted that during the model setup of both predictive tools, the computational time used by the process-based approach was 0.78 times smaller than that used by the ANN approach due to the additional time spent on ANN development (see Fig. 7). Conversely, the computational costs of forecasting are considerably reduced by the ANN models compared with the process-based model, with decreases of 25, 600, 3900, and 31633 times for forecasting 1 h, 1 day, 1 month and 1 bathing season, respectively. Thus, the longer the forecasting period, the greater the reduction in computational time by ANN models.

Therefore, both approaches have advantages for different purposes. The value of the ANN model presented here is that it is very quick to implement and can be used for nowcasting of bathing water quality, whereas a process-based model can be used to investigate processes that govern the levels of *E. coli* in the estuary. Once the ANN model is trained and validated, it can be easily used by bathing water managers to identify potential risks for users, support decision-making tasks and allow administrations to promote preventive management actions.

5. Conclusions

The proposed methodology forecasts FIO concentrations (*E. coli* in this study) and classifies bathing sites for any period, integrating the benefits of laboratory analyses, numerical modelling, and machine learning. Our study demonstrated that the proposed method allows the evolution of FIO concentrations to be calculated for any period at the bathing sites, optimizing the trade-off between computational cost and the result accuracy of conventional process-based models and data-driven models. Thus, ANN models are viable emulators of highly nonlinear process-based models driven by highly variable forcings. However, surrogate validity outside of the training region is difficult to evaluate and should be further researched.

FIO concentrations were the focus here, but the method could be adapted to address the concentration of other water constituents such as total dissolved oxygen, nutrients, suspended sediments, heavy metals, organic micropollutants, and/or microplastics or to predict FIO concentrations in shellfish, with the aim of protecting consumers from faeces-contaminated shellfish.

From a technical perspective, the ANN models have a strong predictive ability for nonlinear systems and can enhance the overall reliability and applicability of process-based models. From the operational perspective, the implementation of ANN models is highly efficient at a very low cost compared to the implementation of process-based models (see subsection 3.3). This capability is particularly useful in scenarios where on-the-spot decisions are needed (e.g., temporary closure of a bathing site), for which the use of complex and detailed process-based models can be cumbersome. Thus, ANN models could be applied in early warning systems for the public to minimize contact with bathing waters impacted by high faecal levels (daily planning of bathing sites). Nevertheless, the accuracy of river flows and meteorological forecasts must be considered for any temporal horizon.

Acknowledgements

The authors would like to thank SAI, CMEMS, MeteoGalicia, and NAYADE for the provided field data, the local treatment plant operator and staff for their forthcoming collaboration, and the editor and reviewers for their suggestions that have improved this article.

References

1. Bárcena, J.F., Claramunt, I., García-Alba, J., Pérez, M.L., García, A., 2017a. A method to assess the evolution and recovery of heavy metal pollution in estuarine sediments: Past history, present situation and future perspectives. Marine Pollution Bulletin 124 (1), 421-434.
2. Bárcena, J.F., Gómez, A.G., García, A., Álvarez, C., Juanes, J.A., 2017b. Quantifying and mapping the vulnerability of estuaries to point-source pollution using a multi-metric assessment: The Estuarine Vulnerability Index (EVI). Ecological Indicators 76, 159-169.
3. Bedri, Z., Corkery, A., O'Sullivan, J.J., Alvarez, M.X., Erichsen, A.C., Deering, L.A., Demeter, K., O'Hare, G.M.P., Meijer, W.G., Masterson, B., 2014. An integrated catchment-coastal modelling system for real-time water quality forecasts. Environmental Modelling and Software 61, 458-476.
4. Bedri, Z., Corkery, A., O'Sullivan, J.J., Deering, L.A., Demeter, K., Meijer, W.G., O'Hare, G., Masterson, B., 2016. Evaluating a microbial water quality prediction model for beach management under the revised EU Bathing Water Directive. Journal of Environmental Management 167, 49-58.
5. Bennett, N.D., Croke, B.F.W., Guariso, G., Guillaume, J.H.A., Hamilton, S.H., Jakeman, A.J., Marsili-Libelli, S., Newham, L.T.H., Norton, J.P., Perrin, C., Pierce, S.A., Robson, B., Seppelt, R., Voinov, A.A., Fath, B.D., Andreassian, V., 2013. Characterising performance of environmental models. Environmental Modelling and Software 40, 1-20.
6. Besmer, M.D., Weissbrodt, D.G., Kratochvil, B.E., Sigrist, J.A., Weyland, M.S., Hammes, F., 2014. The feasibility of automated online flow cytometry for in-situ monitoring of microbial dynamics in aquatic ecosystems. Frontiers in Microbiology 5, 265.

7. Boehm, A.B., 2007. Enterococci Concentrations in Diverse Coastal Environments Exhibit Extreme Variability. Environmental Science and Technology 41 (24), 8227-8232.
8. Boehm, A.B., Grant, S.B., Kim, J.H., Mowbray, S.L., McGee, C.D., Clark, C.D., Foley, D.M., Wellman, D.E., 2002. Decadal and Shorter Period Variability of Surf Zone Water Quality at Huntington Beach, California. Environmental Science and Technology 36 (18), 3885-3892.
9. Bravo, H.R., McLellan, S.L., Val Klump, J., Hamidi, S.A., Talarczyk, D., 2017. Modeling the fecal coliform footprint in a Lake Michigan urban coastal area. Environmental Modelling and Software 95, 401-419.
10. Castelletti, A., Galelli, S., Ratto, M., Soncini-Sessa, R., Young, P.C., 2012. A general framework for Dynamic Emulation Modelling in environmental problems. Environmental Modelling and Software 34, 5-18.
11. Chandramouli, V., Brion, G., Neelakantan, T.R., Lingireddy, S., 2007. Backfilling missing microbial concentrations in a riverine database using artificial neural networks. Water Research 41 (1), 217-227.
12. Chapra, S.C., 1997. Surface Water-Quality Modeling, McGraw-Hill Companies, Inc., USA.
13. de Brauwere, A., Ouattara, N.K., Servais, P., 2014. Modeling fecal indicator bacteria concentrations in natural surface waters: a review. Critical Reviews in Environmental Science and Technology 44 (21), 2380-2453.
14. De los Ríos, A., Echavarri-Erasun, B., Lacorte, S., Sánchez-Ávila, J., De Jonge, M., Blust, R., Orbea, A., Juanes, J. A., Cajaraville, M. P., 2016. Relationships between lines of evidence of pollution in estuarine areas: Linking contaminant levels with

biomarker responses in mussels and with structure of macroinvertebrate benthic communities. Marine Environmental Research 121, 49-63.

15. de Paz, L., Patrício, J., Marques, J.C., Borja, A., Laborda, A.J., 2008. Ecological status assessment in the lower Eo Estuary (Spain). The challenge of habitat heterogeneity integration: A benthic perspective. Marine Pollution Bulletin 56 (7), 1275-1283.
16. del Río, S., Herrero, L., Fraile, R., Penas, A., 2011. Spatial distribution of recent rainfall trends in Spain (1961-2006). International Journal of Climatology 31 (5), 656-667.
17. Diffey, B.L., 2002. Sources and measurement of ultraviolet radiation. Methods 28 (1), 4-13.
18. Directive (2006/7/EC) of the European Parliament and of the Council, of 15 February 2006, concerning the management of bathing water quality, OJ L376/14.
19. Dunn, R.J.K., Zigic, S., Shiell, G.R., 2014. Modelling the dispersion of treated wastewater in a shallow coastal wind-driven environment, Geographe Bay, Western Australia: implications for environmental management. Environmental Monitoring and Assessment 186 (10), 6107-6125.
20. Flor, G., Fernández-Pérez, L.A., Cabrera-Ceñal, R., 1993. Aspectos morfológicos del estuario del Eo. Trabajos de Geología 19, 75-95 (in Spanish).
21. FLTQ, 1990. Análisis de las Condiciones Morfodinámicas de la Ría del Eo - Fase II, Informe Final, Fundación Leonardo Torres Quevedo (FLTQ). Consejería de Medio Rural y Pesca del Principado de Asturias, Oviedo, Spain (in Spanish).
22. García, A., Juanes, J.A., Álvarez, C., Revilla, J.A., Medina, R., 2010. Assesment of the response of a shallow macrotidal estuary to changes in hydrological and

wastewater inputs through numerical modelling. Ecological Modelling 221 (8), 1194-1208.

23. Gronewold, A.D., Wolpert, R.L., 2008. Modeling the relationship between most probable number (MPN) and colony-forming unit (CFU) estimates of fecal coliform concentration. Water Research 42 (13), 3327-3334.
24. Hagan, M.T., Menhaj, M.B., 1994. Training feedforward networks with the Marquardt algorithm. IEEE Transactions on Neural Networks 5 (6), 989-993.
25. He, L., He, Z., 2008. Water quality prediction of marine recreational beaches receiving watershed baseflow and stormwater runoff in southern California, USA. Water Research 42 (10-11), 2563-2573.
26. Højris, B., Christensen, S.C.B., Albrechtsen, H.J., Smith, C., Dahlqvist, M., 2016. A novel, optical, on-line bacteria sensor for monitoring drinking water quality. Scientific Reports 6, 23935.
27. Huang, G., Falconer, R.A., Lin, B., 2017. Integrated hydro-bacterial modelling for predicting bathing water quality. Estuarine, Coastal and Shelf Science 188, 145-155.
28. Jiang, Y., Nan, Z., Yang, S., 2013. Risk assessment of water quality using Monte Carlo simulation and artificial neural network method. Journal of Environmental Management 122, 130-136.
29. Kazemi Yazdi, S., Scholz, M., 2010. Assessing storm water detention systems treating road runoff with an artificial neural network predicting fecal indicator organisms. Water, Air, and Soil Pollution 206 (1-4), 35-47.
30. Keeratipibul, S., Phewpan, A., Lursinsap, C., 2011. Prediction of coliforms and Eschericia coli on tomato fruits and lettuce leaves after sanitizing y using Artificial Neural Networks. LWT - Food Science and Technology 44 (1), 130-138.

31. Khalil, B., Ouarda, T.B.M.J., St-Hilaire, A., 2011. Estimation of water quality characteristics at ungauged sites using artificial neural networks and canonical correlation analysis. Journal of Hydrology 405 (3-4), 277-287.

32. Kim, M., Choi, C.Y., Gerba, C.P., 2008. Source tracking of microbial intrusion in water systems using artificial neural networks. Water Research 42 (4-5), 1308-1314.

33. Lesser, G.R., Roelvink, J.A., van Kester, J.A.T.M., Stelling, G.S., 2004. Development and validation of a three-dimensional morphological model. Coastal Engineering 51 (8-9), 883-915.

34. López, I., Álvarez, C., Gil, J.L., García, A., Bárcena, J.F., Revilla, J.A., 2013. A method for the source apportionment in bathing waters through the modelling of wastewater discharges: Development of an indicator and application to an urban beach in Santander (Northern Spain). Ecological Indicators 24, 334-343.

35. Los, F.J. J., Troost, T.A.A., Van Beek, J.K.L., 2014. Finding the optimal reduction to meet all targets-Applying Linear Programming with a nutrient tracer model of the North Sea. Journal of Marine Systems 131, 91-101.

36. Maier, H.R., Jain, A., Dandy, G.C., Sudheer, K.P., 2010. Methods used for the development of neural networks for the prediction of water resource variables in river systems: Current status and future directions. Environmental Modelling and Software 25 (8), 891-909.

37. Mancini, J.L., 1978. Numerical estimates of coliform mortality rates under various conditions. Journal Water Pollution Control Federation 50 (11), 2477-2484.

38. Manzato, A., 2007. Sounding-derived indices for neural network based short-term thunderstorm and rainfall forecasts. Atmospheric Research 83 (2-4), 349-365.

39. Mas, D.M.L., Ahlfeld, D.P., 2007. Comparing artificial neural networks and regression models for predicting faecal coliform concentrations. Hydrological Sciences Journal 52 (4), 713-731.

40. Metcalf and Eddy, Inc., 2003. Wastewater Engineering: Treatment and Reuse, Revised by G. Tchobanoglous, F.L. Burton, and H.D. Stensel, Mc-Graw-Hill, New York, Fourth Edition.

41. Motamarri, S., Boccelli, D.L., 2012. Development of a neural-based forecasting tool to classify recreational water quality using fecal indicator organisms. Water Research 46 (14), 4508-4520.

42. Nash, J.E., Sutcliffe, J.V., 1970. River flow forecasting through conceptual models part I – A discussion of principles. Journal of Hydrology 10 (3), 282-290.

43. Piedracoba, S., Souto, C., Gilcoto, M., Pardo, P.C., 2005. Hydrography and dynamics of the Ría de Ribadeo (NW Spain), a wave driven estuary. Estuarine, Coastal and Shelf Science 65 (4), 726-738.

44. Postma, L., Boderie, P., van Gils, J., van Beek, J., 2003. Component software system for surface water simulations. Lecture Notes in Computer Science 2657, 649-658.

45. Roberts, P.J.W., Villegas, B., 2017. Modeling and Design of the Buenos Aires Outfalls. Journal of Hydraulic Engineering 143 (2), 05016007.

46. Rompré, A., Servais, P., Baudart, J, Renée-de-Roubin, M, Laurent, P., 2002. Detection and enumeration of coliforms in drinking water: current methods and emerging approaches. Journal of Microbiological Methods 49, 31-54.

47. Rumelhart, D.E., Hinton, G.E., William, R.J., 1986. Learning representation by back-propagating errors. Nature 323, 533-536.

48. Schmidhuber, J., 2015. Deep Learning in neural networks: An overview. Neural Networks 61, 85-117.

49. Shaw, A.R., Smith Sawyer, H., LeBoeuf, E.J., McDonald, M.P., Hadjerioua, B., 2017. Hydropower Optimization Using Artificial Neural Network Surrogate Models of a High-Fidelity Hydrodynamics and Water Quality Model. Water Resources Research 53 (11), 9444-9461.

50. Sotillo, M.G., Cailleau, S., Lorente, P., Levier, B., Aznar, R., Reffray, G., Amo-Baladrón, A., Chanut, J., Benkiran, M., Alvarez-Fanjul, E., 2015 The MyOcean IBI Ocean Forecast and Reanalysis Systems: operational products and roadmap to the future Copernicus Service. Journal of Operational Oceanography 8 (1), 63-79.

51. Thoe, W., Gold, M., Griesbach, A., Grimmer, M., Taggart, M.L., Boehm, A.B., 2014. Predicting water quality at Santa Monica Beach: Evaluation of five different models for public notification of unsafe swimming conditions. Water Research 67, 105-117.

52. Thoe, W., Wong, S.H.C., Choi, K.W., Lee, J.H.W., 2012. Daily prediction of marine beach water quality in Hong Kong. Journal of Hydro-Environment Research 6 (3), 164-180.

53. Tufail, M., Ormsbee, L., Teegavarapu, R., 2008. Artificial Intelligence-Based Inductive Models for Prediction and Classification of Fecal Coliform in Surface Waters. Journal of Environmental Engineering 134 (9), 789-799.

54. van der Merwe, R., Leen, T.K., Lu, Z., Frolov, S., Baptista, A.M., 2007. Fast neural network surrogates for very high dimensional physics-based models in computational oceanography. Neural Networks 20 (4), 462-478.

55. Vang, O.K., Corfitzen, C.B., Smith, C., Albrechtsen, H-J., 2014. Evaluation of ATP measurements to detect microbial ingress by wastewater and surface water in drinking water. Water Research 64, 309-320.

56. Walker, D.I., McQuillan, J., Taiwo, M., Parks, R., Stenton, C.A., Morgan, H., Mowlem, M.C., Lees, D.N., 2017. A highly specific Escherichia coli qPCR and its comparison with existing methods for environmental waters. Water Research 126, 101-110.

57. Wang, X., Zhang, J., Babovic, V., 2016. Improving real-time forecasting of water quality indicators with combination of process-based models and data assimilation technique. Ecological Indicators 66, 428-439.

58. Washington, W.M., Buja, L., Craig, A., 2009. The computational future for climate and earth system models: on the path to petaflop and beyond. Philosophical Transactions of the Royal Society Academy Series A 367 (1890), 833-846.

59. Wu, W., Dandy, G.C., Maier, H.R., 2014. Protocol for developing ANN models and its application to the assessment of the quality of the ANN model development process in drinking water quality modelling. Environmental Modelling and Software 54, 108-127.

60. Zhang, Z., Deng, Z., Rusch, K.A., 2015. Modeling Fecal Coliform Bacteria Levels at Gulf Coast Beaches. Water Quality, Exposure and Health 7 (3), 255-263.

61. Zou, R., Lung, W-S., Wu, J., 2007. An adaptive neural network embedded genetic algorithm approach for inverse water quality modeling. Water Resources Research 43 (8), W08427.

Figure and Table captions

Fig. 1. Map of the Eo River Basin and the Eo Estuary, indicating the locations of the tidal gauges (TG1-TG4), monitoring points (MP1-MP3), flow gauge (FG1), meteorological station (MS1), bathing water quality control points (BP1-BP4), and faecal discharges (FD1-FD3) used in the setup of the predictive tools. Bathymetry is also presented with a zoomed-in image of the outer and inner areas of the Eo Estuary (UTM projection ED50 30N).

Fig. 2. Schematic view of a feedforward neural network with five nodes in the input layer, three nodes in the hidden layer and one node in the output layer. Synapses are oriented from left to right.

Fig. 3. Overall methodological approach.

Fig. 4. Schematic view of the proposed methodology to develop artificial neural networks to analyse bathing water quality criteria in estuaries.

Fig. 5. Performance of the final artificial neural networks (outputs) in emulating *E. coli* concentrations (*E. coli*/100 ml) computed by the process-based model (targets) at BP1 (a), BP2 (b), BP3 (c), and BP4 (d). The bias, R^2, and CE magnitudes are also shown for the four bathing sites (BP1-BP4). The colorbar shows the occurrence probability of the scatter dots defined by the *E. coli* concentration of targets (process-based model) and outputs (ANN model).

Fig. 6. Performance of the process-based model (filled markers) and the ANN models (unfilled markers) in simulating the *E. coli* concentrations (*E. coli*/100 ml) at BP1 (squares), BP2 (circles), BP3 (diamonds), and BP4 (triangles) during the bathing season of 2013 (red), 2014 (green), and 2015 (blue). The bias, R^2, and CE magnitudes are also shown for the four bathing sites (BP1-BP4) and considering all the bathing seasons and locations at the same time (global).

Fig. 7. Computational times required to simulate FIO concentrations by the process-based model and by the ANN model using the proposed methodology. Note that Forecasting: 1 h, Forecasting: 1 day, Forecasting: 1 month, and Forecasting: 1 bathing season refer to the simulation times.

Table 1. (a): Contingency table used to assess the accuracy of predictive tools for the prediction of faecal indicator organism (FIO) concentrations. (b): Error metrics of the contingency table (Source: Manzato, 2007; Bennett et al., 2013; Bedri et al. 2016).

Table 2. Model parameters used in the calculation of *E. coli* transport and mixing.

Table 3. Computed metrics for the assessment of the accuracy of the predictive tools in predicting compliance with/exceedance of the *E. coli* values of 500, 250, 125, 50, and 25 *E. coli*/100 ml.

Table 4. Review of previous research predicting faecal indicator organisms (FIOs) with multilayer feedforward networks consisting of one input layer, one hidden layer, and one output layer.

		Observed Exceedances: yes	Observed Exceedances: no	
Predicted Exceedances	yes	Hits	False alarms	Predicted yes
	no	Misses	Correct negatives	Predicted no
		Observed yes	Observed no	Total

a) Contingency table

Metric	Formula	Range of values	Ideal value	Notes
Accuracy (fraction correct)	$\frac{Hits + Correct\ negatives}{Total}$	0-1	1	It is heavily influenced by the most common category, usually “no event”.
Bias score (frequency bias)	$\frac{Hits + False\ alarms}{Hits + Misses}$	0-∞	1	Indicates if the model tends to under- (<1) or over- (>1) estimate.
Hit rate (Probability of detection)	$\frac{Hits}{Hits + Misses}$	0-1	1	Sensitive to hits but ignores false alarms. Good for rare events.
False alarm rate (Probability of false detection)	$\frac{False\ alarms}{False\ alarms + Correct\ negatives}$	0-1	0	Sensitive to false alarms but ignores misses.
Success index	$\frac{1}{2}\cdot\left[\frac{Hits}{Hits + Misses} + \frac{Correct\ negatives}{Total}\right]$	0-1	1	Weights equally the ability of the model to correctly detect occurrences and non-occurrences of events.
Threat score	$\frac{Hits + Correct\ negatives}{Total}$	0-1	1	Measures the fraction of observed cases that were correctly modelled. It penalizes both misses and false alarms.

b) Error metrics

Constant	Value	Units	Source
D_H, D_V	Time series	m^2/s	Hydrodynamic module
T	Time series	ºC	Hydrodynamic module
C_{Cl}	Time series	g/m^3	Hydrodynamic module
I_0	Time series	W/m^2	Meteorological station (MS1)
K_B	0.8	1/days	Chapra (1997)
DL	1	days	(*)
f_{uv}	0.12	-	Diffey (2002)
ε	0.35	1/m	FLTQ (1990); Eq. (5)
K_T	1.07	-	This study (calibration)
k_{rd}	0.086	$m^2/W{\cdot}days$	This study (calibration)
k_{Cl}	$2{\cdot}10^{-4}$	$m^3/g{\cdot}days$	This study (calibration)

(*) Day-night variations are considered within the irradiation (I_0).

Bathing site	Contingency table (metrics)	Value = 500 *E. coli*/100 ml		Value = 250 *E. coli*/100 ml		Value = 125 *E. coli*/100 ml		Value = 50 *E. coli*/100 ml		Value = 25 *E. coli*/100 ml	
		Process-based	ANN	Process-based	ANN	Process-based	ANN	Process-based	ANN	Process-based	ANN
BP1	Accuracy	1.00	1.00	1.00	1.00	1.00	1.00	1.00	1.00	1.00	1.00
	Bias score	(*)	(*)	(*)	(*)	(*)	(*)	1.00	1.00	1.00	1.00
	Hit rate	(*)	(*)	(*)	(*)	(*)	(*)	1.00	1.00	1.00	1.00
	False alarm rate	0.00	0.00	0.00	0.00	0.00	0.00	0.00	0.00	0.00	0.00
	Success index	(*)	(*)	(*)	(*)	(*)	(*)	0.92	0.92	0.92	0.92
	Threat score	(*)	(*)	1.00	1.00	1.00	1.00	1.00	1.00	1.00	1.00
BP2	Accuracy	1.00	1.00	0.88	0.88	0.96	1.00	0.96	0.92	0.96	0.84
	Bias score	(*)	(*)	1.33	1.33	0.86	1.00	1.09	1.00	0.93	0.78
	Hit rate	(*)	(*)	0.67	0.67	0.86	1.00	1.00	0.92	0.93	0.78
	False alarm rate	0.00	0.00	0.09	0.09	0.00	0.00	0.07	0.08	0.00	0.00
	Success index	(*)	(*)	0.73	0.73	0.79	0.88	0.76	0.70	0.67	0.53
	Threat score	(*)	(*)	0.88	0.88	0.96	1.00	0.96	0.92	0.96	0.84
BP3	Accuracy	1.00	1.00	0.96	0.96	0.88	0.96	0.77	0.92	0.88	0.96
	Bias score	(*)	(*)	0.00	0.00	0.25	0.50	0.85	0.82	0.83	0.94
	Hit rate	(*)	(*)	0.00	0.00	0.25	0.50	0.69	0.82	0.83	0.94
	False alarm rate	0.00	0.00	0.00	0.00	0.00	0.00	0.15	0.00	0.00	0.00
	Success index	(*)	(*)	0.48	0.48	0.55	0.71	0.56	0.68	0.56	0.62
	Threat score	(*)	(*)	0.96	0.96	0.88	0.96	0.77	0.92	0.88	0.96
BP4	Accuracy	1.00	1.00	1.00	1.00	0.92	1.00	0.90	0.73	0.91	0.83
	Bias score	(*)	(*)	1.00	1.00	0.33	1.00	0.78	0.78	0.88	0.88
	Hit rate	(*)	(*)	1.00	1.00	0.33	1.00	0.78	0.56	0.88	0.82
	False alarm rate	0.00	0.00	0.00	0.00	0.00	0.00	0.00	0.15	0.00	0.17
	Success index	(*)	(*)	0.98	0.98	0.60	0.98	0.67	0.53	0.57	0.52
	Threat score	(*)	(*)	1.00	1.00	0.92	1.00	0.90	0.73	0.91	0.83

(*) Indeterminate form 0/0.

Study	**FIO(*)**	n_i	n_h	f_h**(**)**	f_o**(**)**	**Training method**	n_e	$T:V:T$	R^2
Chandramouli et al. (2007)	FC	7	9	Log	Log	Back-propagation	(***)	75:15:10	0.63-0.94
Mas and Ahlfeld (2007)	FC	6	16	Tan	Tan	Levenberg-Marquardt	10^3	64:16:20	(***)
Kim et al. (2008)	EC	3	1	Tan	Tan	Back-propagation	$5{\cdot}10^4$	72:8:20	0.90-0.96
He and He (2008)	TC	7	3	(***)	(***)	Back-propagation	(***)	56:24:20	0.79
He and He (2008)	FC	12	6	(***)	(***)	Back-propagation	(***)	56:24:20	0.82
He and He (2008)	EN	7	8	(***)	(***)	Back-propagation	(***)	56:24:20	0.86
Tufail et al. (2008)	EC	2	4	Log	Log	Back-propagation	10^4	80:20:(***)	0.58-0.73
Kazemi Yazdi and Scholz (2010)	EN	4	8	Tan	Tan	Levenberg-Marquardt	10^3	65:15:20	0.15-0.80
Keeratipibul et al. (2011)	EC	6	5	Tan	Log	Back-propagation	(***)	70:30:(***)	0.72
Thoe et al. (2012)	FC	7	5	Log	Lin	Gradient-descent with momentum	10^3	60:20:20	0.29-0.75
Motamarri and Boccelli, (2012)	FC	5	6	Tan	Lin	Levenberg-Marquardt	10^3	99:1 (leave-one-out)	(***)
Thoe et al. (2014)	FC	12	5	Log	Lin	Gradient-descent	$2{\cdot}10^4$	60:20:20	0.38-0.58
Zhang et al. (2015)	FC	14	(***)	(***)	(***)	Back-propagation	(***)	60:20:20	0.68
This study (2018)	EC	9	15	Tan	Log	Levenberg-Marquardt	10^3	70:15:15	0.55-0.75

(*) FC: *Faecal coliform*, TC: *Total coliform*, EC: *E. coli*, EN: *Intestinal enterococci.*
(**) Log: Log-sigmoid, Tan: Tan-sigmoid, Lin: Linear.
(***) Non-specified in the study.

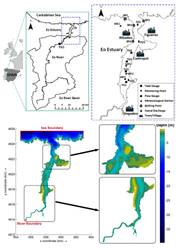

SPAIN
Cantabrian Sea
Eo Estuary
FG1
Eo River
Eo River Basin
0 5 10 20 Km
BP1
BP2
FD2
MS1
BP3
Ribadeo
Figueras
BP4
FD3
Eo Estuary
TG4
Castropol
TG3
MP3
TG2
MP2
MP1
FD1
TG1
Tidal Gauge
Monitoring Point
Flow Gauge
Meteorological Station
Bathing Point
Faecal Discharge
Town/Village
Vegadeo
Sea Boundary
River Boundary
y coordinate (km) →
x coordinate (km) →
Depth (m)

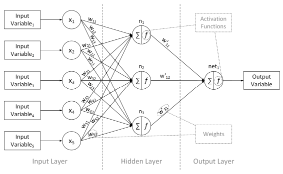

Input Variable1
Input Variable2
Input Variable3
Input Variable4
Input Variable5
x1
x2
x3
x4
x5
w11
w12
w13
w21
w22
w23
w31
w32
w33
w41
w42
w43
w51
w52
w53
n1
n2
n3
w'11
w'12
w'31
net1
Activation Functions
Weights
Output Variable
Input Layer
Hidden Layer
Output Layer

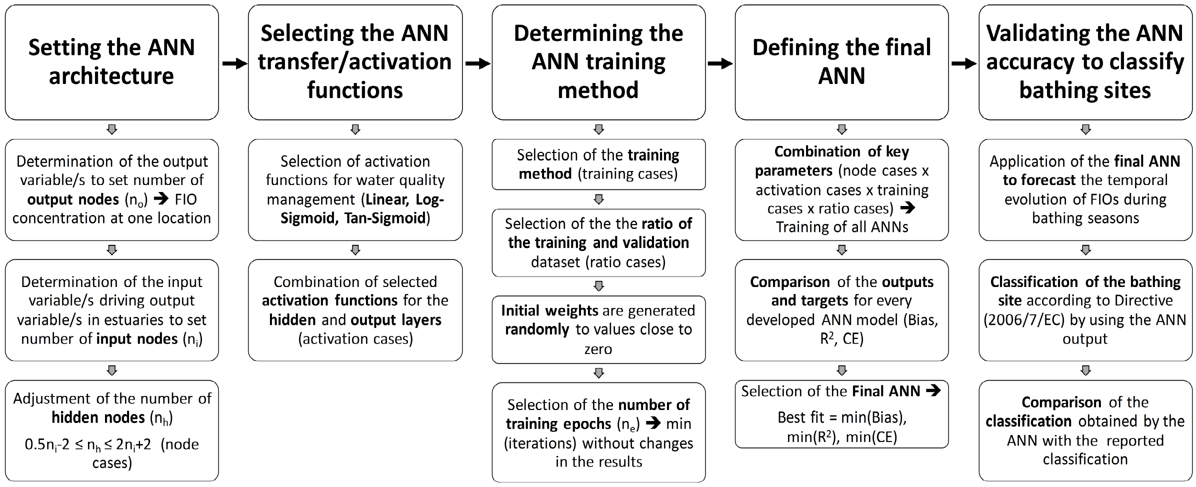
Setting the ANN architecture
Determination of the output variable/s to set number of output nodes (n_o) ➔ FIO concentration at one location
Determination of the input variable/s driving output variable/s in estuaries to set number of input nodes (n_i)
Adjustment of the number of hidden nodes (n_h)
$0.5n_i-2 \leq n_h \leq 2n_i+2$ (node cases)
Selecting the ANN transfer/activation functions
Selection of activation functions for water quality management (Linear, Log-Sigmoid, Tan-Sigmoid)
Combination of selected activation functions for the hidden and output layers (activation cases)
Determining the ANN training method
Selection of the training method (training cases)
Selection of the the ratio of the training and validation dataset (ratio cases)
Initial weights are generated randomly to values close to zero
Selection of the number of training epochs (n_e) ➔ min (iterations) without changes in the results
Defining the final ANN
Combination of key parameters (node cases x activation cases x training cases x ratio cases) ➔ Training of all ANNs
Comparison of the outputs and targets for every developed ANN model (Bias, R^2, CE)
Selection of the Final ANN ➔
Best fit = min(Bias), min(R^2), min(CE)
Validating the ANN accuracy to classify bathing sites
Application of the final ANN to forecast the temporal evolution of FIOs during bathing seasons
Classification of the bathing site according to Directive (2006/7/EC) by using the ANN output
Comparison of the classification obtained by the ANN with the reported classification

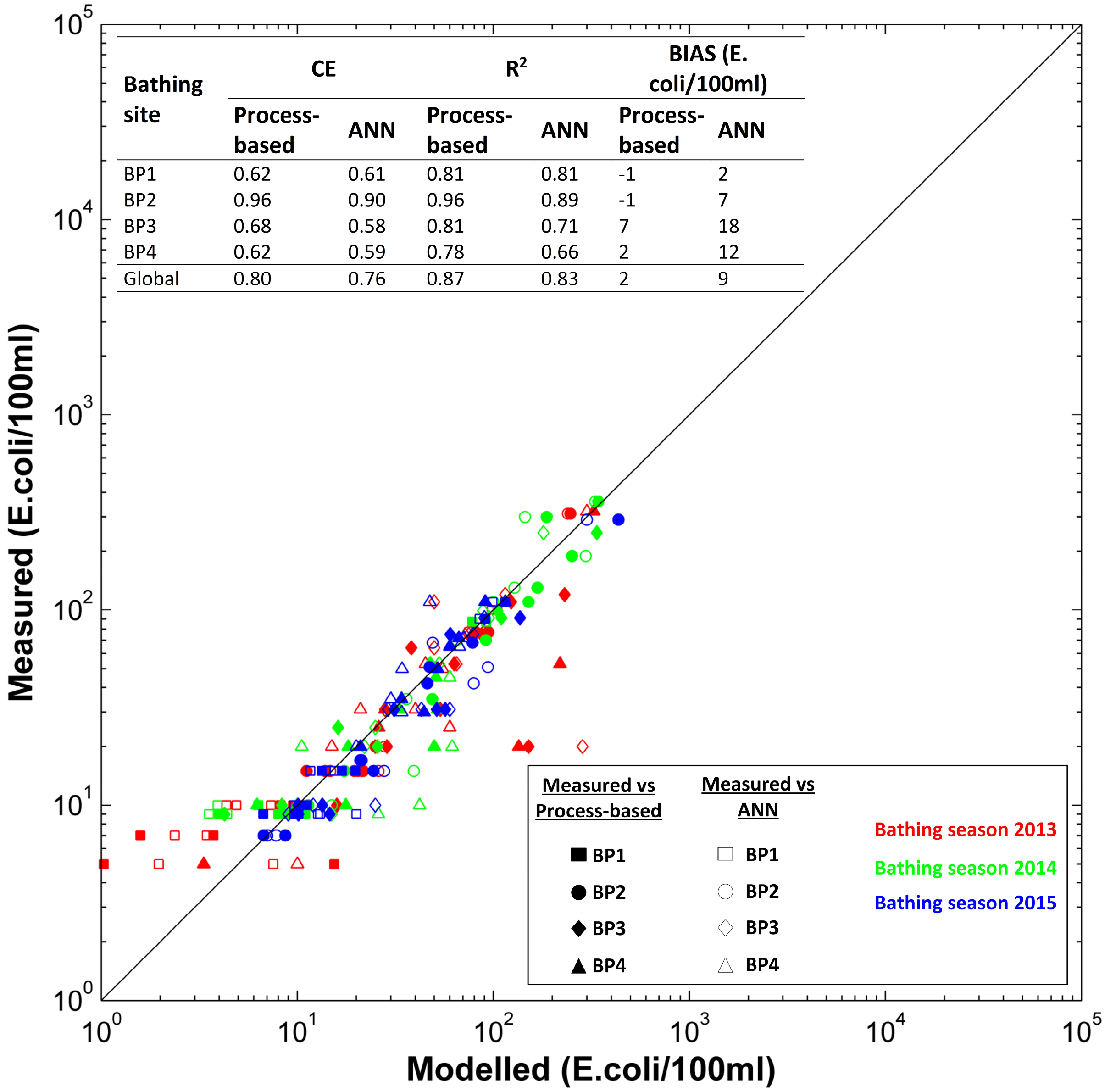

Bathing site
CE
R2
BIAS (E. coli/100ml)
Process-based
ANN
BP1 0.62 0.61 0.81 0.81 -1 2
BP2 0.96 0.90 0.96 0.89 -1 7
BP3 0.68 0.58 0.81 0.71 7 18
BP4 0.62 0.59 0.78 0.66 2 12
Global 0.80 0.76 0.87 0.83 2 9
Measured vs Process-based
Measured vs ANN
BP1
BP2
BP3
BP4
Bathing season 2013
Bathing season 2014
Bathing season 2015
Measured (E.coli/100ml)
Modelled (E.coli/100ml)
10^0
10^1
10^2
10^3
10^4
10^5

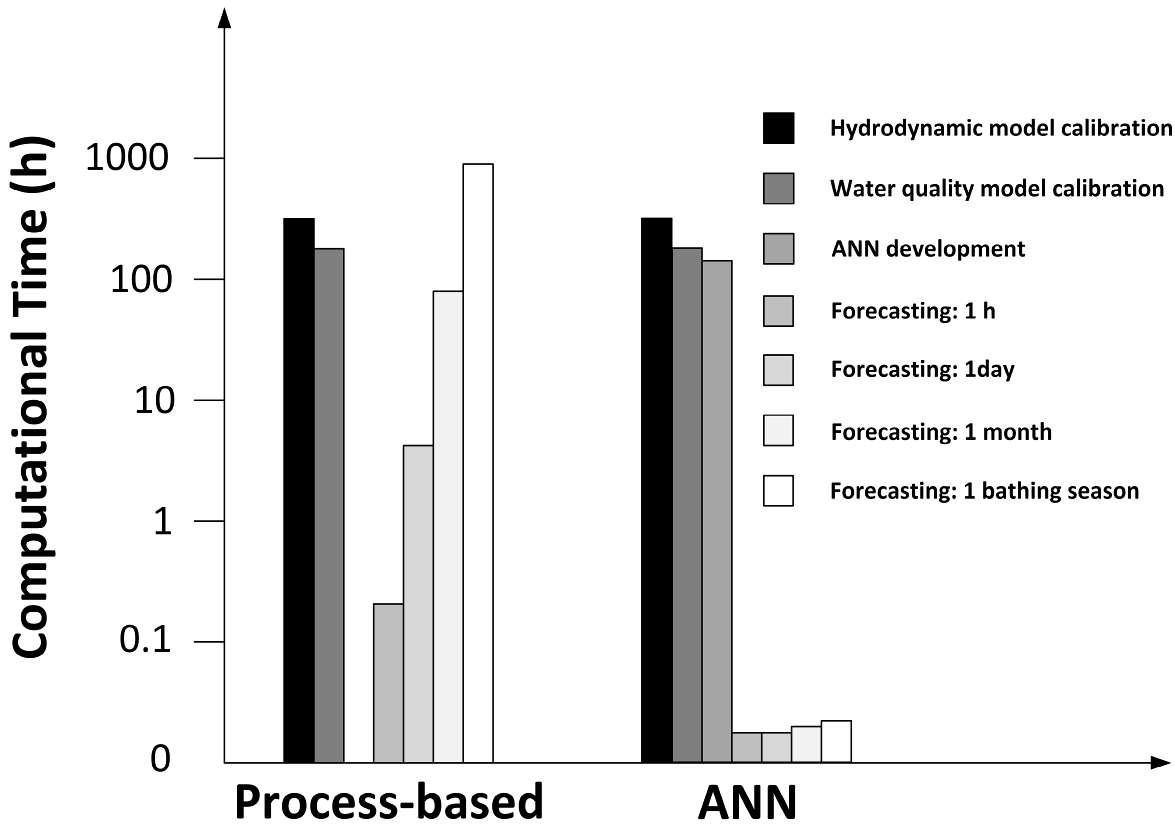

Computational Time (h)
1000
100
10
1
0.1
0
Process-based
ANN
Hydrodynamic model calibration
Water quality model calibration
ANN development
Forecasting: 1 h
Forecasting: 1day
Forecasting: 1 month
Forecasting: 1 bathing season

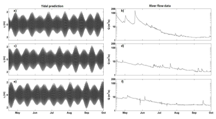
Tidal prediction
River flow data
a)
b)
c)
d)
e)
f)
η (m)
Q (m³/s)
May
Jun
Jul
Aug
Sep
Oct

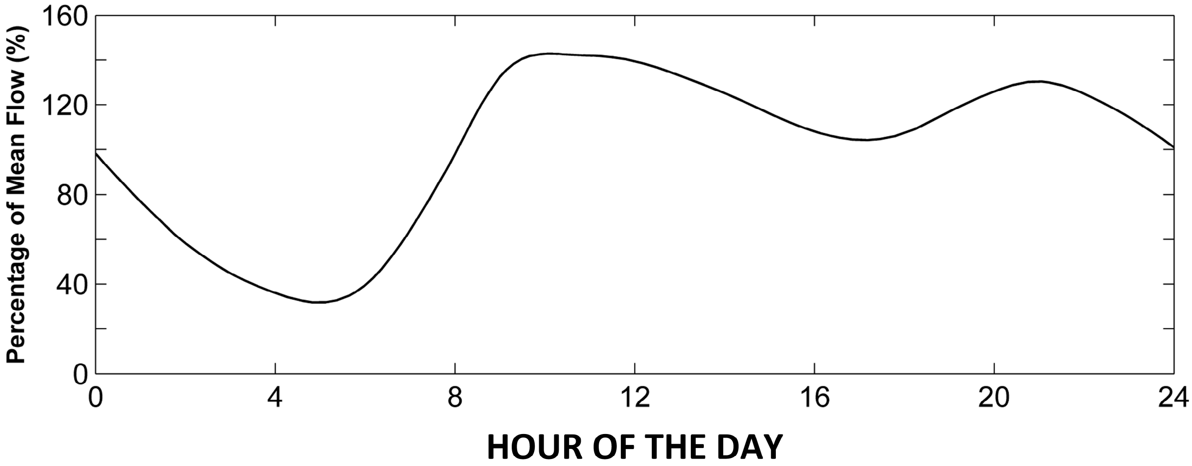
Percentage of Mean Flow (%)
160
120
80
40
0
0
4
8
12
16
20
24
HOUR OF THE DAY

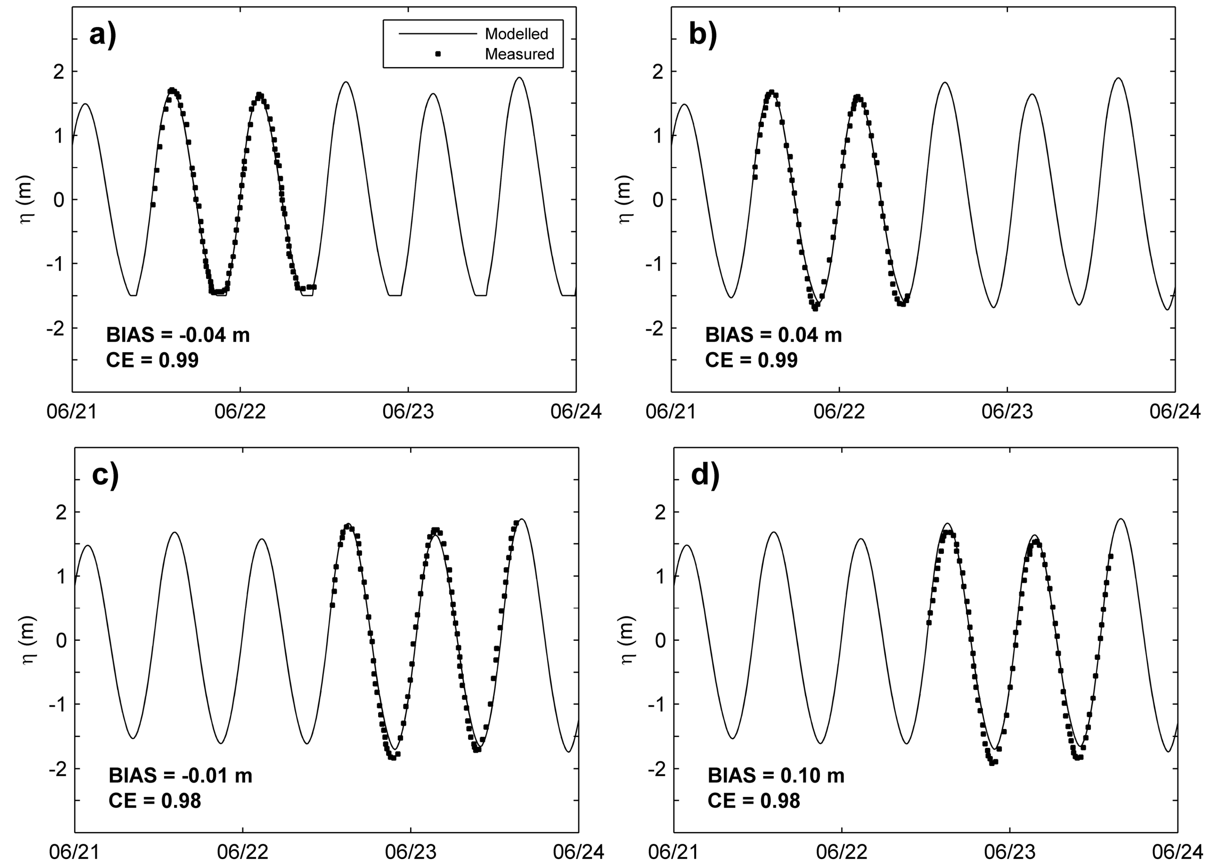
a)
Modelled
Measured
BIAS = -0.04 m
CE = 0.99
b)
BIAS = 0.04 m
CE = 0.99
c)
BIAS = -0.01 m
CE = 0.98
d)
BIAS = 0.10 m
CE = 0.98
η (m)
06/21
06/22
06/23
06/24

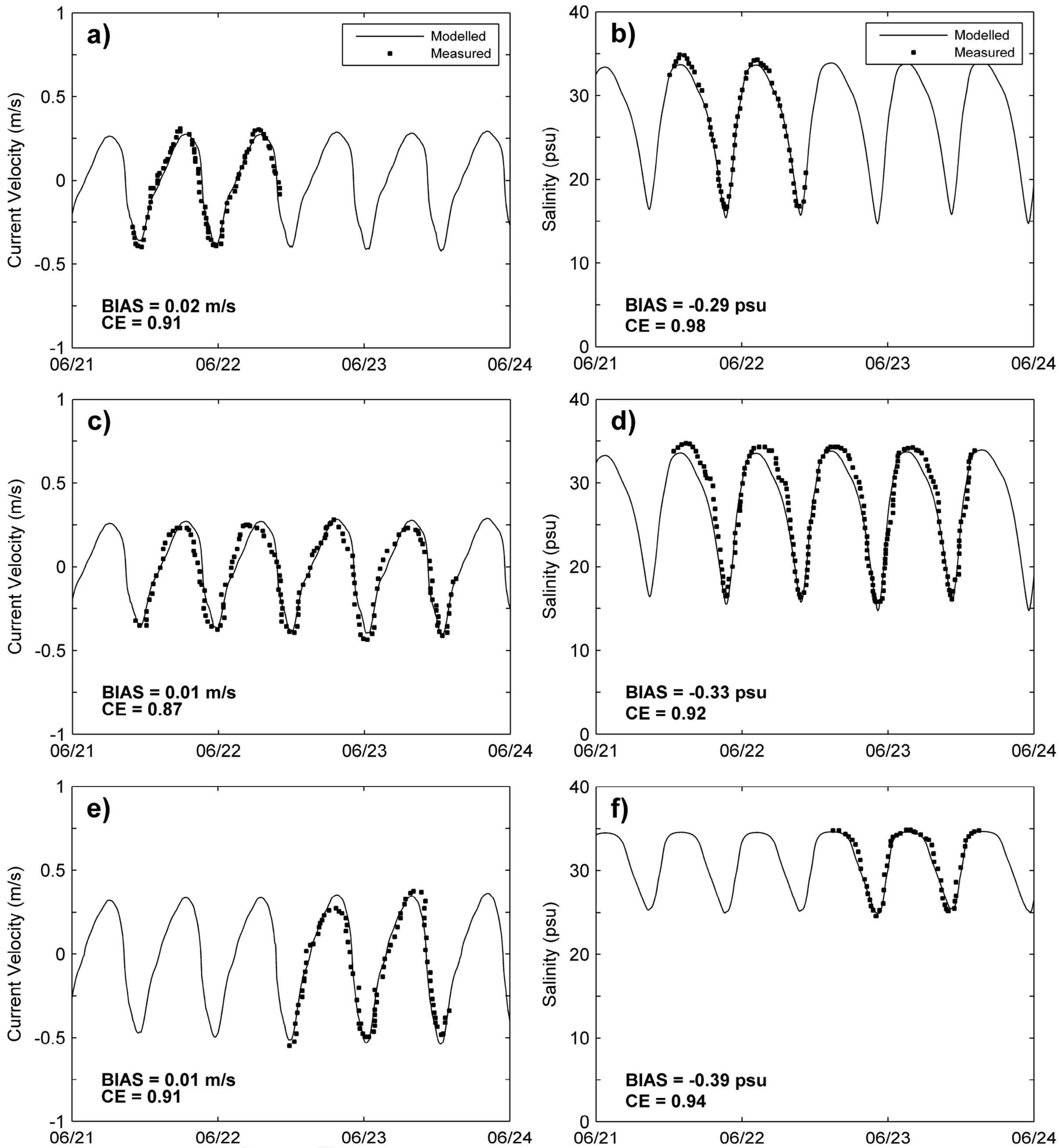
a)
Modelled
Measured
Current Velocity (m/s)
BIAS = 0.02 m/s
CE = 0.91
b)
Modelled
Measured
Salinity (psu)
BIAS = -0.29 psu
CE = 0.98
c)
Current Velocity (m/s)
BIAS = 0.01 m/s
CE = 0.87
d)
Salinity (psu)
BIAS = -0.33 psu
CE = 0.92
e)
Current Velocity (m/s)
BIAS = 0.01 m/s
CE = 0.91
f)
Salinity (psu)
BIAS = -0.39 psu
CE = 0.94
06/21
06/22
06/23
06/24

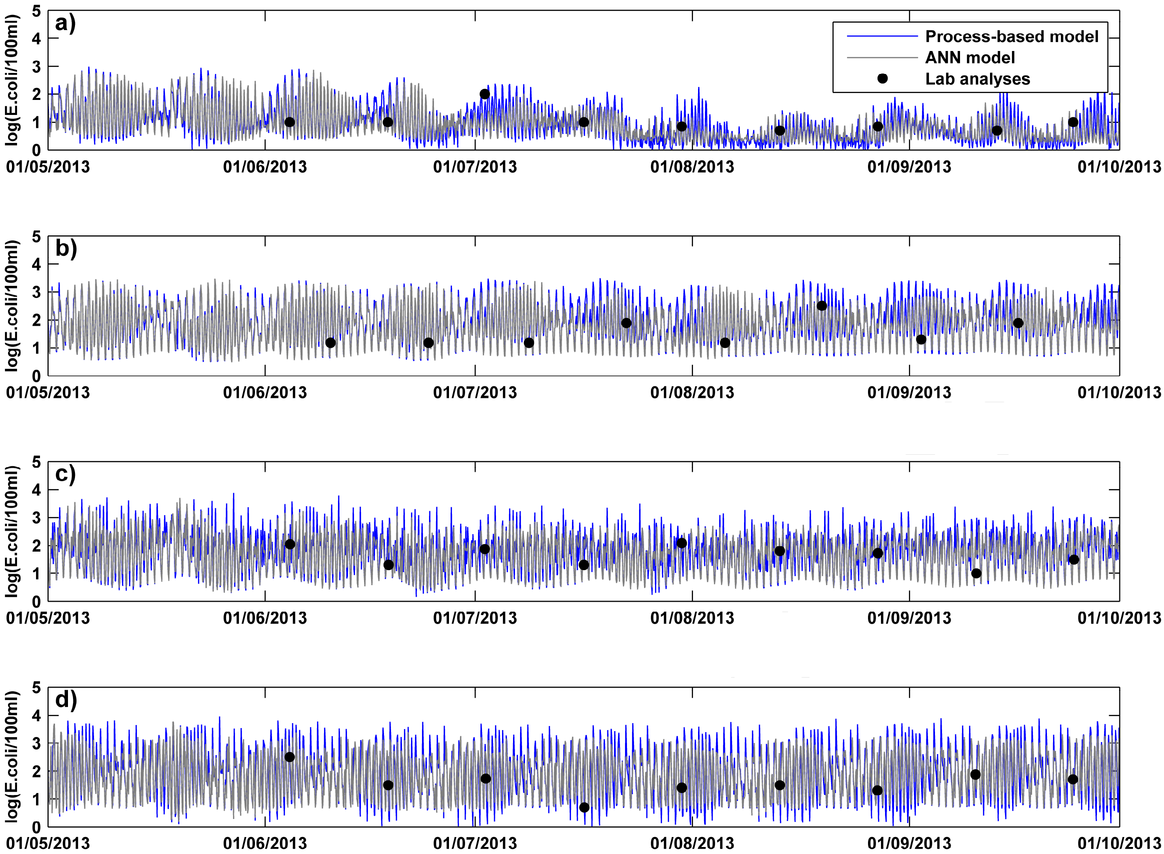
a)
b)
c)
d)
log(E.coli/100ml)
0
1
2
3
4
5
Process-based model
ANN model
Lab analyses
01/05/2013
01/06/2013
01/07/2013
01/08/2013
01/09/2013
01/10/2013

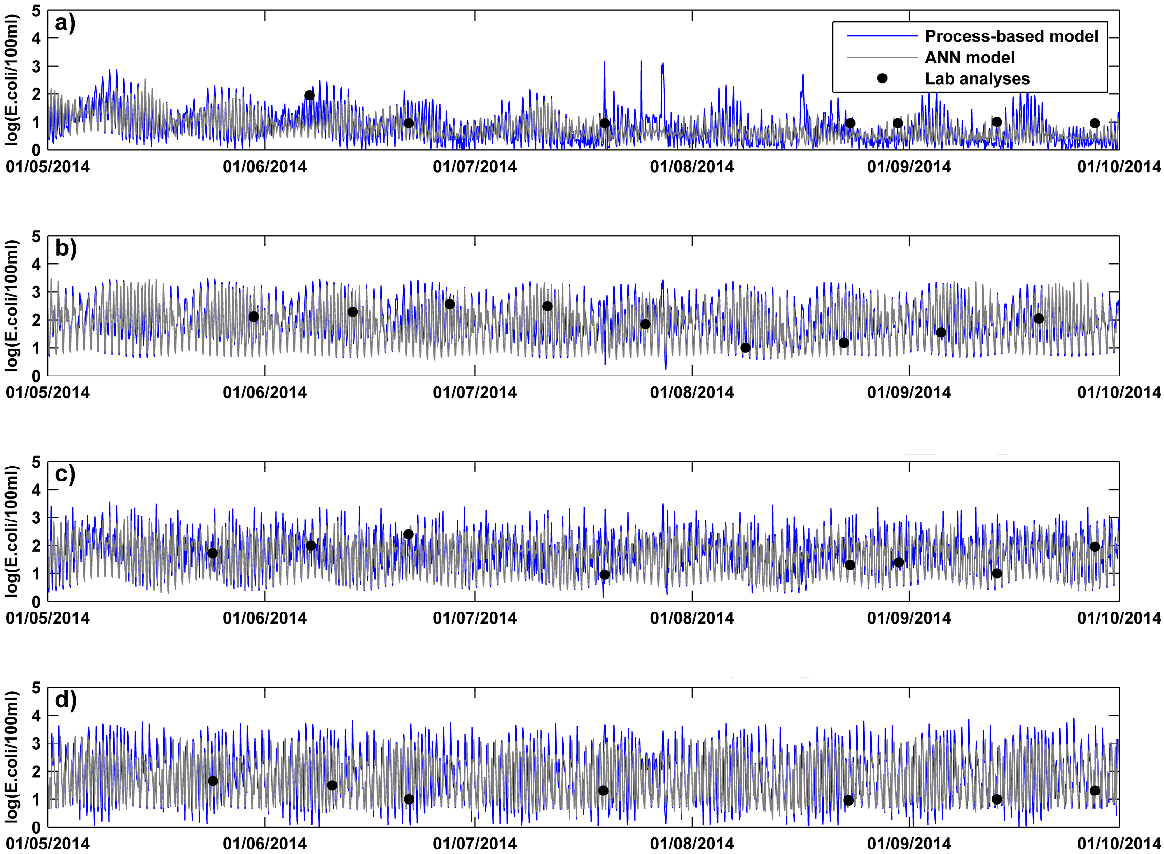

a)
b)
c)
d)
Process-based model
ANN model
Lab analyses
log(E.coli/100ml)
0
1
2
3
4
5
01/05/2014
01/06/2014
01/07/2014
01/08/2014
01/09/2014
01/10/2014

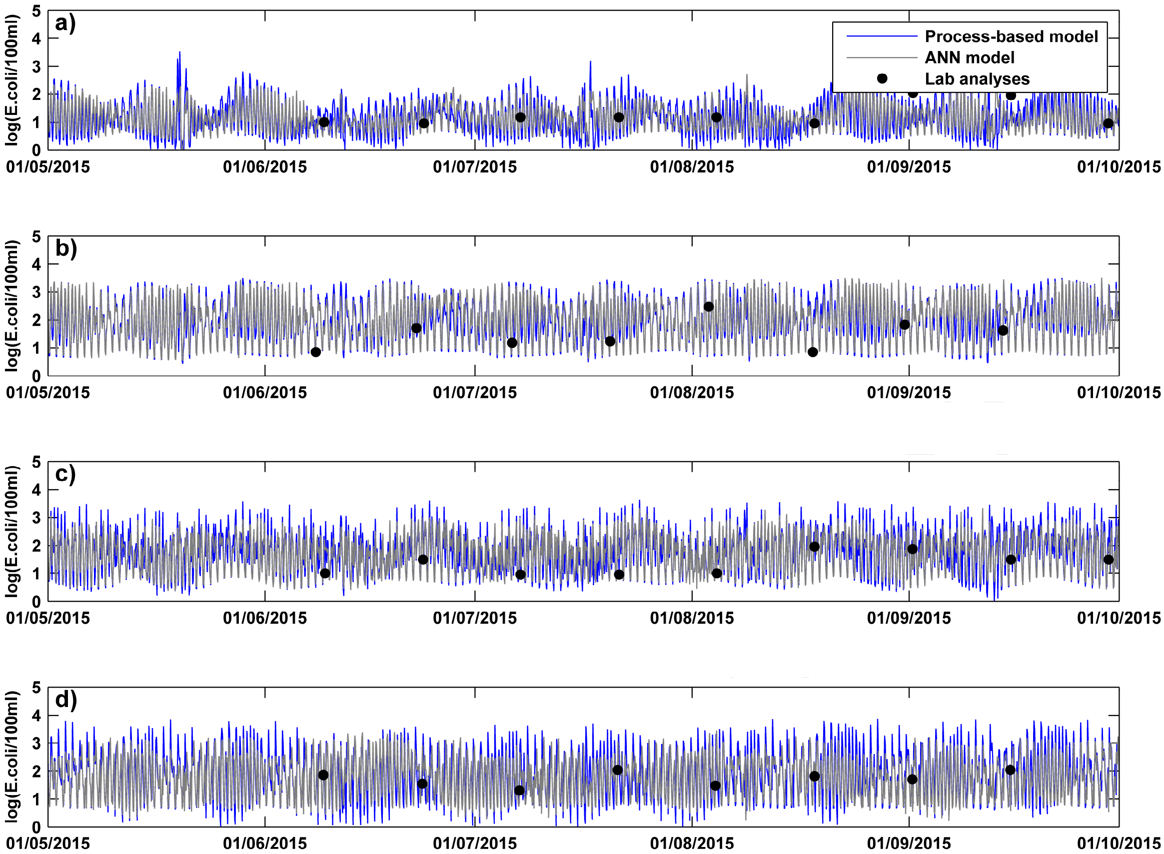
a)
b)
c)
d)
log(E.coli/100ml)
0
1
2
3
4
5
Process-based model
ANN model
Lab analyses
01/05/2015
01/06/2015
01/07/2015
01/08/2015
01/09/2015
01/10/2015

- The method integrates laboratory analyses, numerical modelling and machine learning.
- ANN configuration for predicting *E. coli* concentration in estuaries is determined.
- ANNs are viable emulators of process-based models driven by highly variable forcing.
- The longer forecasting, the greater the reduction in computational time using ANN.
- Real-time management of bathing water quality is enabled by using ANNs.

Declaration of interests

☒ The authors declare that they have no known competing financial interests or personal relationships that could have appeared to influence the work reported in this paper.

☐The authors declare the following financial interests/personal relationships which may be considered as potential competing interests: